Dynamics of Track Deflection Associated with the Passage of Tropical Cyclones over a Mesoscale Mountain

YUH-LANG LIN AND NICHOLAS C. WITCRAFT

Department of Marine, Earth, and Atmospheric Sciences, North Carolina State University, Raleigh, North Carolina

YING-HWA KUO

Mesoscale and Microscale Meteorology Division, National Center for Atmospheric Research, Boulder, Colorado

(Manuscript received 9 August 2005, in final form 21 February 2006)

ABSTRACT

In this study, the fifth-generation Pennsylvania State University–National Center for Atmospheric Research (PSU–NCAR) Mesoscale Model (MM5) was used to simulate Supertyphoon Bilis (in 2000) and Typhoon Toraji (in 2001) in order to investigate the dynamics of track deflection caused by the Central Mountain Range (CMR) of Taiwan. The MM5 predicted the track of each storm reasonably well. Bilis was stronger and had a relatively faster forward motion, which helped make the track continuous as it crossed the CMR. The use of a "bogus" vortex in the initialization process helped produce a storm closer to the observed strength. Bilis is a classic example of a typhoon crossing Taiwan with a continuous track. For comparison, Typhoon Toraji, a typical typhoon having a discontinuous track, was also studied. Toraji was weaker and had a relatively slower forward speed, which prevented the original low center from crossing over the CMR and forced more air parcels to go around the northern tip of the CMR. As a result, it produced a vortex and a secondary low center on the lee. Potential vorticity banners on the north side of the CMR acted to organize the secondary low and the lee vortex. With time, the low-level circulation extended into the upper levels, completing the formation of the secondary center. Remnants of the initial center crossed over the CMR and were entrained into the secondary center. Nondimensional control parameters for track continuity and deflection from idealized studies are calculated for Bilis and Toraji. The results are consistent with the theory proposed in Lin et al. For tropical cyclones (TCs) approaching Taiwan from the southeast, the conceptual model proposed by Lin et al. for continuous and discontinuous tracks was applied. For continuous tracks over the CMR, the blocking effect on the outer circulation of the vortex is weak and the vorticity advection around the northern tip is strong due to an intense TC. Weak TCs tend to be totally blocked by the CMR.

1. Introduction

Taiwan is extremely vulnerable to the passage of tropical cyclones (TCs). In a typical year, three to four typhoons passed over the island nation, with one or two making landfall. However, a typhoon does not need to make direct landfall for Taiwan to experience damaging winds and heavy rains. The forecasting of typhoons around Taiwan is complicated by the rugged topography of Taiwan's Central Mountain Range (CMR), which has an average elevation of 3000 m, a north–south length of about 300 km, and, an east–west width of about 100 km. The isolated nature of Taiwan makes it an ideal environment for research into the orographic effects on tropical cyclones.

There are a number of past studies concerning the orographic influence on the tracks of TCs passing over not only Taiwan but also the islands of Cuba, Hispañiola, and Puerto Rico in the Caribbean, and Luzon in the Phillipines. Lin (1993) and Wu and Kuo (1999) provided synopses of previous work on typhoons affecting Taiwan. Wang (1980) and Brand and Blelloch (1974) found that some typhoons took a cyclonic track when passing over Taiwan. Stronger typhoons tended to have a continuous track (Fig. 1a). On the contrary, weaker typhoons tended to "jump" over the island by forming a secondary circulation center on the lee side,

Corresponding author address: Dr. Yuh-Lang Lin, Dept. MEAS, North Carolina State University, 1125 Jordan Hall, Faucette Dr., Raleigh, NC 27695-8208.
E-mail: yl_lin@ncsu.edu

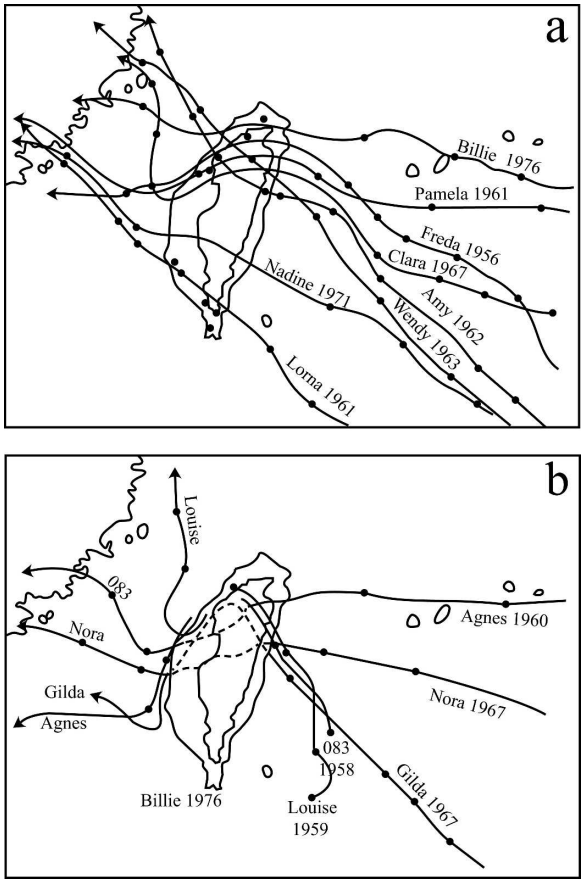

FIG. 1. (a) Paths of selected typhoons that had a continuous track around Taiwan. Also shown is the terrain of Taiwan, with contours every 1000 m. (b) Paths of selected weak typhoons that had a discontinuous track over Taiwan. The original centers were blocked by the Central Mountain Range, replaced by secondary centers on the lee side. (Adapted from Wang 1980.)

with the original center being blocked by the terrain, making the track discontinuous (Fig. 1b). The secondary center may develop and eventually replace the parent typhoon. Chang (1982) verified these observational studies with one of the first idealized modeling studies of typhoons passing over Taiwan. Further idealized simulations (Bender et al. 1985, 1987; Yeh and Elsberry 1993a,b; Huang and Lin 1997; Lin et al. 1999, 2002) have been made over the years. A drawback of these studies is the failure to resolve the finescale terrain features of Taiwan, which may dictate how and where mesoscale vortices and lows will form in the lee of the CMR.

As numerical models are improved, a few real-case modeling studies have been made. For example, Wu (2001) used the Geophysical Fluid Dynamics Laboratory (GFDL) hurricane model to study the interaction of Typhoon Gladys with the Taiwan terrain. Gladys experienced a southward deflection and deceleration upon approach to Taiwan similar to that seen in some of the idealized studies (e.g., Lin et al. 1999). After crossing Taiwan, Gladys accelerated to the northwest. The weakening of Gladys during its landfall on Taiwan was underestimated, which was due primarily to the cutoff of the supply of water vapor in the boundary layer. Though the orographic precipitation was underpredicted, the overall distribution and the locations of the precipitation maxima were well simulated. The location of the secondary mesolows also matched observations fairly well. The mesolow located east of the mountains was shown to be caused by downslope adiabatic warming (foehn) associated with the circulation of Gladys, and helped to pull the low center slightly southwestward when it crossed Taiwan. A potential vorticity (PV) budget analysis showed that condensational heating plays a significant role in the evolution of PV as the storm crosses Taiwan. Surface dissipation of PV was important when Gladys was crossing over Taiwan. Lin et al. (2002) adopted the Naval Research Laboratory's Coupled Ocean–Atmosphere Mesoscale Prediction System (COAMPS) model to simulate Supertyphoon Bilis (2000) to examine the dynamics of orographic rainfall and track deflection associated with the storm as it passed over the CMR of Taiwan. The track of the model typhoon was found to be discontinuous, while the observed track was continuous. This is likely due to the lack of implanting a "bogus" vortex at the initialization time, causing the storm to be too weak at landfall. The model storm and the observed storm were deflected northward before landfall, and then back southward afterward, consistent with previous studies. Jian et al. (2006) performed numerical simulations of Typhoon Dot (1990), which had a discontinuous track, and found that the merge of the adiabatically induced low and the secondary vortex formed by vorticity stretching on the lee side dominated the low-level development of the surface vortex while the midlevel cyclone was still located on the upstream of CMR. This low-level vortex then coupled vertically with the midlevel vortex after passing over the CMR and redeveloped to a mature typhoon. In this study, we will focus on studying the control parameters and mechanisms responsible for track deflection and discontinuity, and the organization of secondary low and lee vortex. In addition, Yang and Ching (2005) have applied the control parameters proposed by Lin et al. (2005, hereafter LCHH) to their simulation results of Typhoon Toraji and found the westward track discontinuity is consistent with LCHH's theory.

In this paper we will closely analyze two different storms: Supertyphoon Bilis (in 2000) and Typhoon

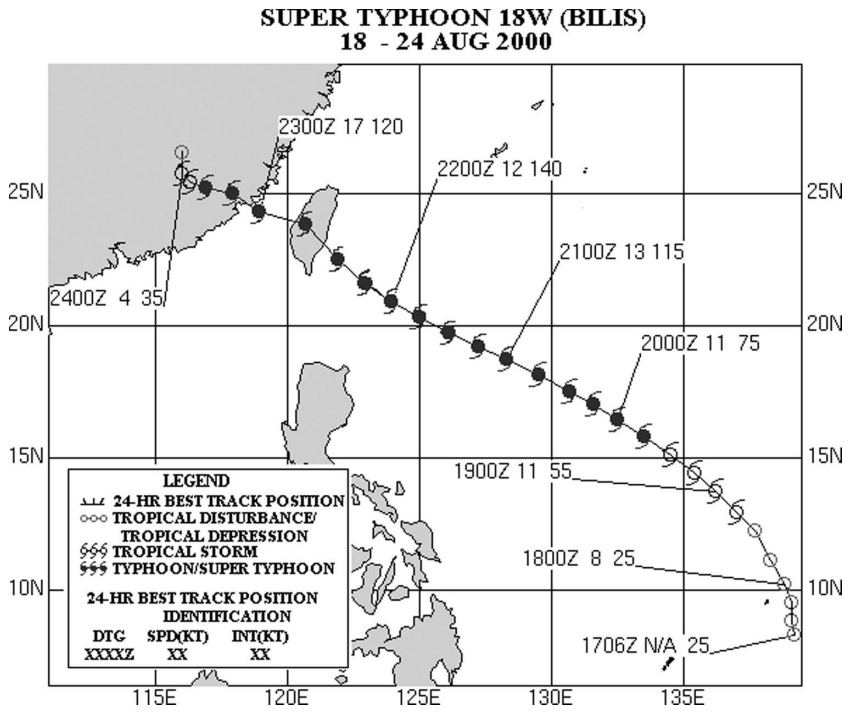

FIG. 2. Track of Supertyphoon Bilis (in 2000) from the Joint Typhoon Warning Center (JTWC).

Toraji (in 2001). Bilis was near supertyphoon strength when it hit the southeast coast of Taiwan and was a typical typhoon having a continuous track over Taiwan. Typhoon Toraji was of moderate intensity and had a slower translation speed as it hit central-east Taiwan. Toraji was a typical typhoon having a discontinuous track over Taiwan. The goal of this study is to use a high-resolution numerical model to investigate the dynamics of track deflection by a mesoscale mountain. In addition, we will test LCHH's theory of control parameters for cyclone track deflection and continuity over a mesoscale mountain to Bilis and Toraji. The theory will be briefly reviewed in section 5.

This paper is organized as follows. Section 2 will discuss the synoptic and mesoscale environments and the configuration of the fifth-generation Pennsylvania State University–National Center for Atmospheric Research (PSU–NCAR) Mesoscale Model (MM5) model simulations. Section 3 will describe briefly the model characteristics and experiment design. In section 4, we will discuss model results and investigate the mechanisms controlling a continuous and discontinuous track. In section 5, we will briefly review LCHH's theory on the control parameters for track continuity and deflection for TCs passing over Taiwan and evaluate the applicability of their theory to Supertyphoon Bilis and Typhoon Toraji. Concluding remarks are made in section 6.

2. Synopses of Supertyphoon Bilis and Typhoon Toraji

a. Synopsis of Supertyphoon Bilis

Supertyphoon Bilis (in 2000) formed as a tropical depression northwest of Yap Island at 1200 UTC 18 August 2000. It followed an almost straight northwesterly track approaching Taiwan and was a very intense category-5 typhoon with a minimum pressure of 915 mb as it made landfall on the southeast coast of Taiwan near Tai-Tung (23.1°N, 121.4°E) around 1400 UTC 22 August 2000. The best track from the Joint Typhoon Warning Center (JTWC) is shown in Fig. 2. The storm produced a maximum wind of 70 m s^{-1} and heavy rainfall of 949 mm in 20 h measured at Yu-Li in eastern Taiwan. Several people died or were seriously injured by landslides triggered by the heavy rainfall. Just before landfall, Bilis turned northward and followed a cyclonic track across the island, which is similar to many previously observed and simulated TCs passing over Taiwan (Fig. 1a). A well-defined eye of Bilis was noticeable as it approached Taiwan, as can be seen on satellite imagery (Lin et al. 2002). After the landfall over Taiwan it weakened rapidly. It then continued to move westward and made landfall on the southeast coast of China around 1200 UTC 12 August 2000. The high terrain of the CMR helped weaken Bilis significantly.

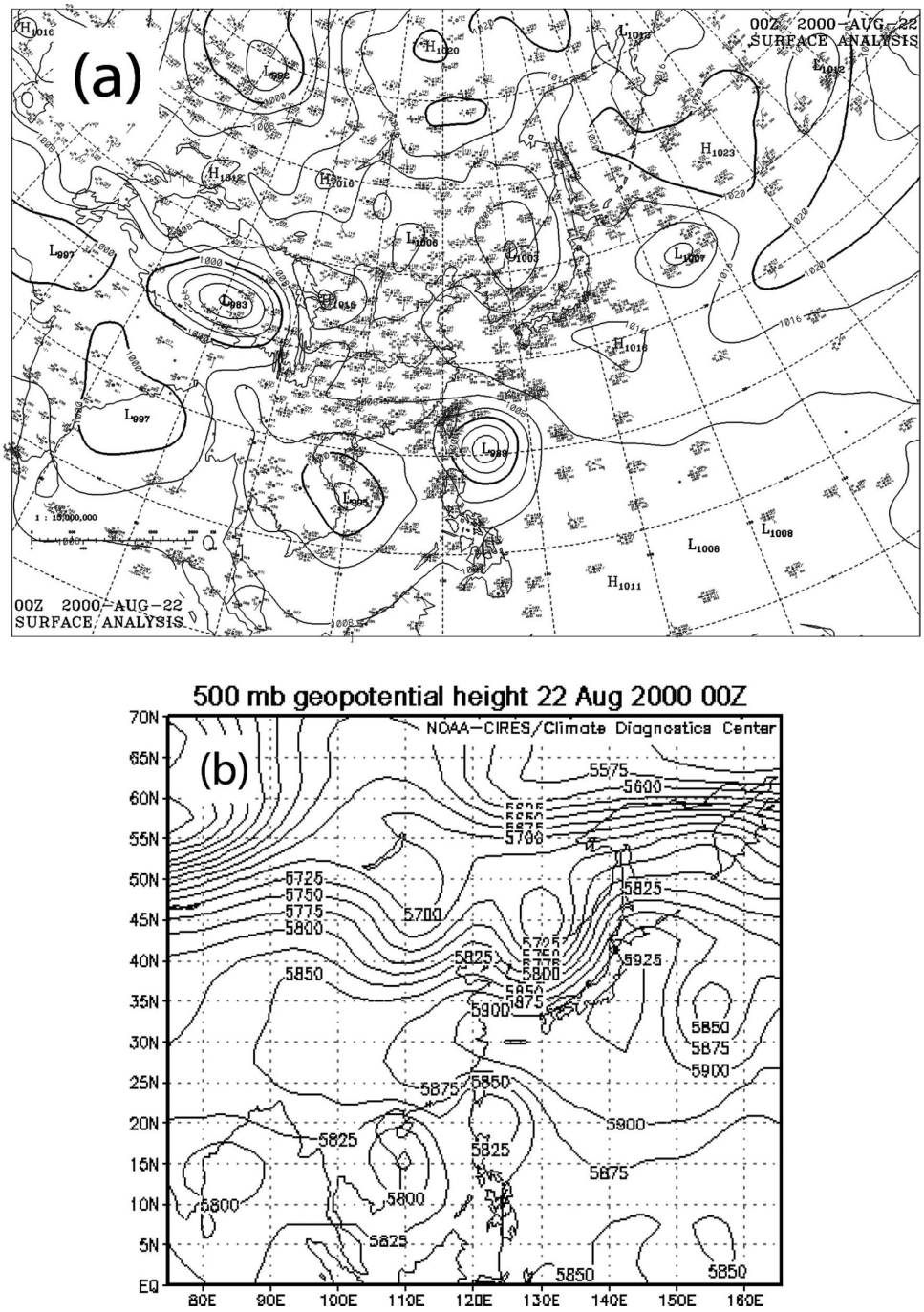

FIG. 3. (a) Surface analysis (hPa), and (b) 500-mb geopotential height (m) field for Supertyphoon Bilis at 0000 UTC 22 Aug 2000. Panel (a) is from Japan Meteorological Agency (JMA), while (b) is generated by NOAA–CDC.

Figure 3a shows the observed synoptic environment across eastern Asia and the northwestern Pacific Ocean at 0000 UTC 22 August 2000. Another tropical system, Tropical Storm Kaemi, was near the central coast of Vietnam, and made landfall 12 h later and dissipated inland on the Indo-China Peninsula. North and northeast of Bilis there was a persistent, but spatially small, area of high pressure systems that moved generally westward. These high pressure systems, along with Tropical Storm Kaemi and the north Pacific high, tended to help advect or steer Bilis northwestward toward Taiwan. There were no significant midlatitude

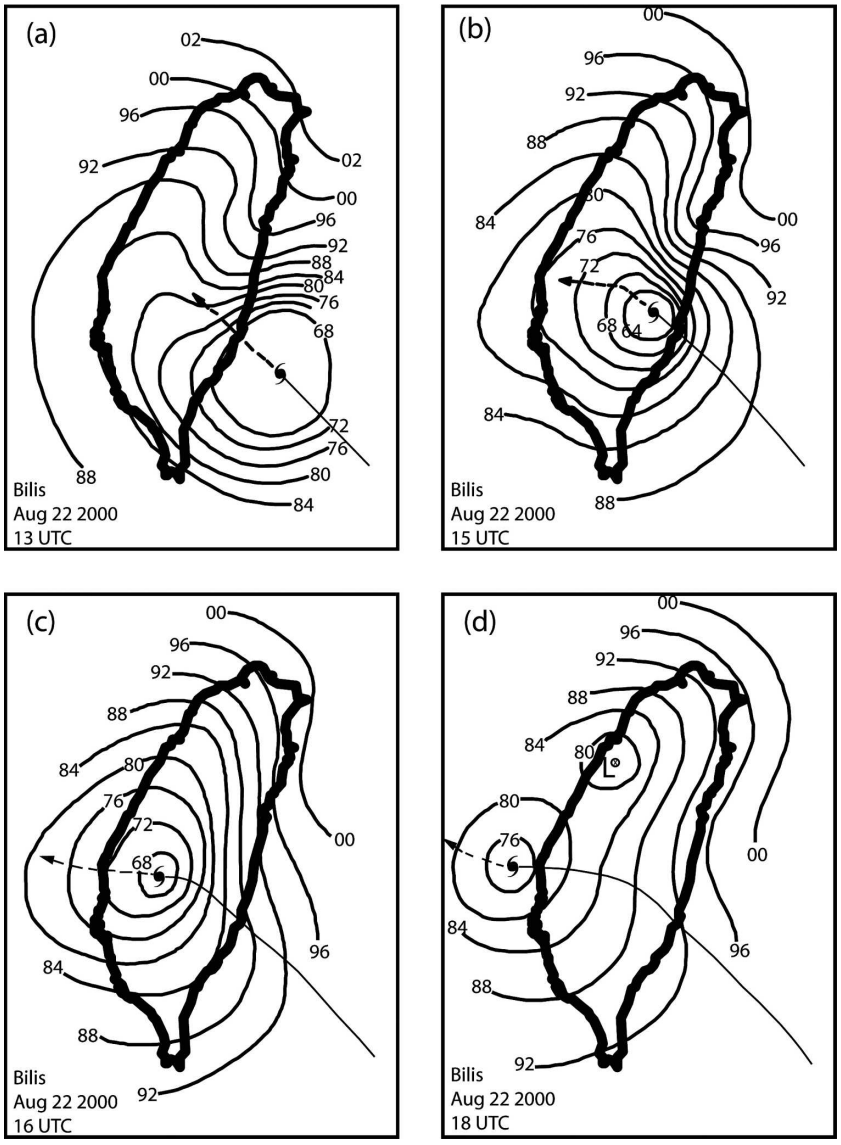

FIG. 4. Surface analysis for Bilis (in 2000) from the CWB. Times are indicated on the figures. Values between 00 to 49 indicate pressure between 1000 and 1049 hPa. Values between 50 and 99 indicate pressure between 950 and 999 hPa.

weather systems in the area to influence the track and rainfall of Bilis. The 500-mb chart (Fig. 3b) shows an upper-level high pressure centered halfway between Taiwan and Japan, with a ridge extending to the east and west. This persistent system helped steer Bilis to the northwest toward Taiwan, and also shielded Bilis from the trough to the north.

The Taiwan Central Weather Bureau (CWB) mesoscale analysis (Fig. 4) provides a good indication as to what happened at landfall. At 1300 UTC 22 August 2000 (Fig. 4a), Bilis was approaching the southeast coast of Taiwan. In the northern lee of the CMR, latent heating and adiabatic warming created an area of lower pressure. This low pressure in the lee persisted during the next 3 h (Figs. 4b,c) as the center crossed the CMR. An inverted ridge (trough) was produced to the northeast (northwest) of the CMR before Bilis passed over the CMR (Figs. 4a,b) due to orographic forcing. Only after the center emerges off the western coast was a closed secondary center evident in the lee of Taiwan (Fig. 4d).

b. Synopsis of Typhoon Toraji

Typhoon Toraji was upgraded from a tropical storm status at 1800 UTC 27 July 2001 when its center was located approximately 700 km southeast of the south-

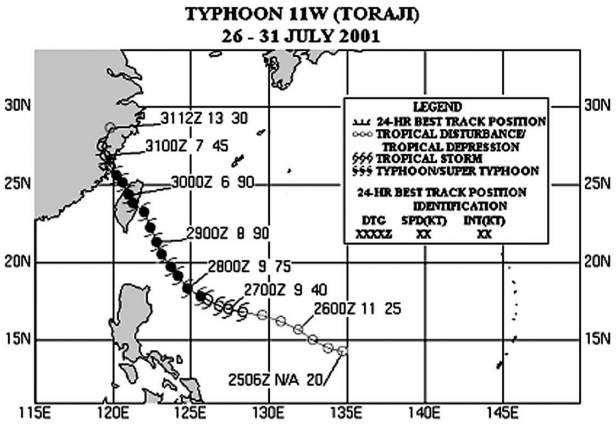

FIG. 5. Track of Typhoon Toraji (in 2001) from CWB.

ern tip of Taiwan. Toraji formed in a weakening subtropical ridge. Initially the TC moved westward and then followed a general northwesterly to north-northwesterly track (Fig. 5) similar to that of Bilis but slightly to the north and slower. The maximum intensity was reached a few hours prior to landfall. The maximum wind was about 49 m s^{-1} and the minimum pressure reported was 960 mb when Toraji made landfall on the southeast coast of Taiwan 1800 UTC 29 July 2001. The initial center of Toraji moved into the CMR and filled in while a new center formed on the northwest coast. The new center moved out into the Taiwan Strait by 0600 UTC 30 July 2001. The interaction with the CMR and the reformation of the center left Toraji disorganized as it crept toward China, as can be seen on satellite and radar imagery (not shown). The maximum rainfall recorded was 686 mm in 35 h in southwest Taiwan. Toraji produced a death toll of 72 and caused the most destruction in Taiwan in nearly four decades since Typhoon Gloria, which left 312 dead in its wake in 1963. Most of the deaths were due to landslides and mudslides triggered by the heavy orographic rainfall.

The surface synoptic conditions at 0000 UTC 29 July 2001 are shown in Fig. 6. An area of weak high pressure is located south and east of Toraji, with general ridging extending north to Japan. Another area of weak high pressure is also located over northern China. A low pressure with a trailing cold front is moving northeastward to the east of China. However, the front does not appear to have much influence on Toraji. At 500 mb (Fig. 6b), a ridge in excess of 590 dam is located to the south of Japan, and to the northeast of Toraji. Toraji appears to be steered around the western periphery of this ridge. There is an extension of the ridge to the north of Toraji.

The differences in the track of Toraji versus Bilis can be seen in the CWB mesoanalyses (Fig. 7). A secondary low and vortex have already formed in the lee of CMR before Toraji made landfall (Fig. 7a) and no secondary vortex formed during the landfall of Bilis (Fig. 4a). The primary storm center crosses the CMR and weakens, while the secondary low and vortex center begins to strengthen (Figs. 7b,c). By 2300 UTC 29 July 2001 (Fig. 7d), the secondary center has taken over as the main center of Toraji.

3. Model description and experiment design

To study Supertyphoon Bilis and Typhoon Toraji numerically, we used version 3 of the MM5 (MM5.v3) model. The model solves the fully compressible, nonhydrostatic governing equations in the σ–z vertical coordinates. Details of the model can be found in Grell et al. (1994). The 1-km resolution terrain and land-use data used in this study provides a much higher terrain resolution than that used in most previous studies.

The National Centers for Environmental Prediction (NCEP) operational analysis with a resolution of 2.5° × 2.5° latitude–longitude and 15 standard pressure layers is used for model initialization and for boundary conditions during model integration. The Bilis experiment is integrated for a period of 48 h from 1200 UTC 21 August to 1200 UTC 23 August 2000. The Toraji experiment is run for a period of 48 h from 1200 UTC 28 July to 1200 UTC 30 July 2001. Because the initial data is too coarse to properly capture a tropical cyclone, the vortices are removed from the analysis and bogus vortices of 70 and 55 m s^{-1} for Bilis and Toraji, respectively, are implanted using the bogussing scheme of Low-Nam and Davis (2001).

There are three nested horizontal domains designed for the simulations (Fig. 8a). Domain 1 has 200 × 200 grid points with a 21-km resolution, domain 2 has 199 × 199 grid points with a 7-km resolution, and domain 3 has 265 × 244 grid points with a 2.33-km resolution. The terrain for domain 3 is shown in Fig. 8b. There are 33 stretched σ levels used with higher resolution in the boundary layer. The top of the model is at 50 mb. The time steps for domains 1, 2, and 3 are 30, 10, and 3.3 s, respectively.

The Blackadar scheme (see Grell et al. 1994) is used to parameterize the planetary boundary layer (PBL) processes including surface fluxes and friction (Zhang and Anthes 1982). The Goddard Lin–Farley–Orville (Lin et al. 1983) scheme (Tao and Simpson 1993) is used to parameterize the microphysical processes in all domains. For domain 1, the Betts–Miller (Betts and Miller 1993) scheme is used to parameterize the subgrid-scale convection, while no cumulus parameterization is used at 7- and 2.3-km resolution simulations.

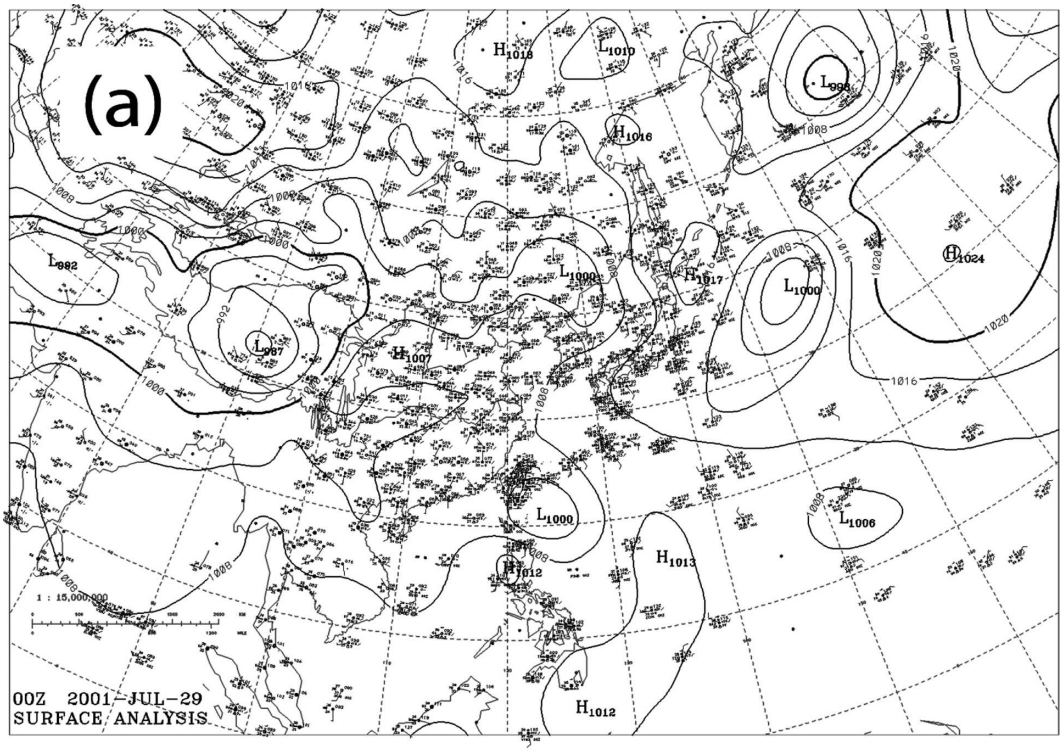

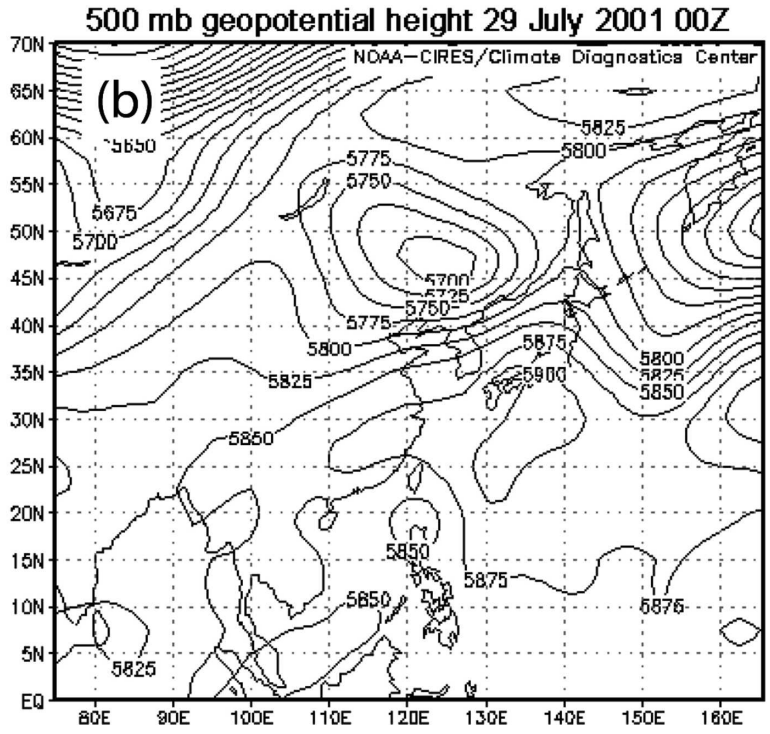

FIG. 6. Same as in Fig. 3, but for Toraji at 0000 UTC 29 Jul 2001.

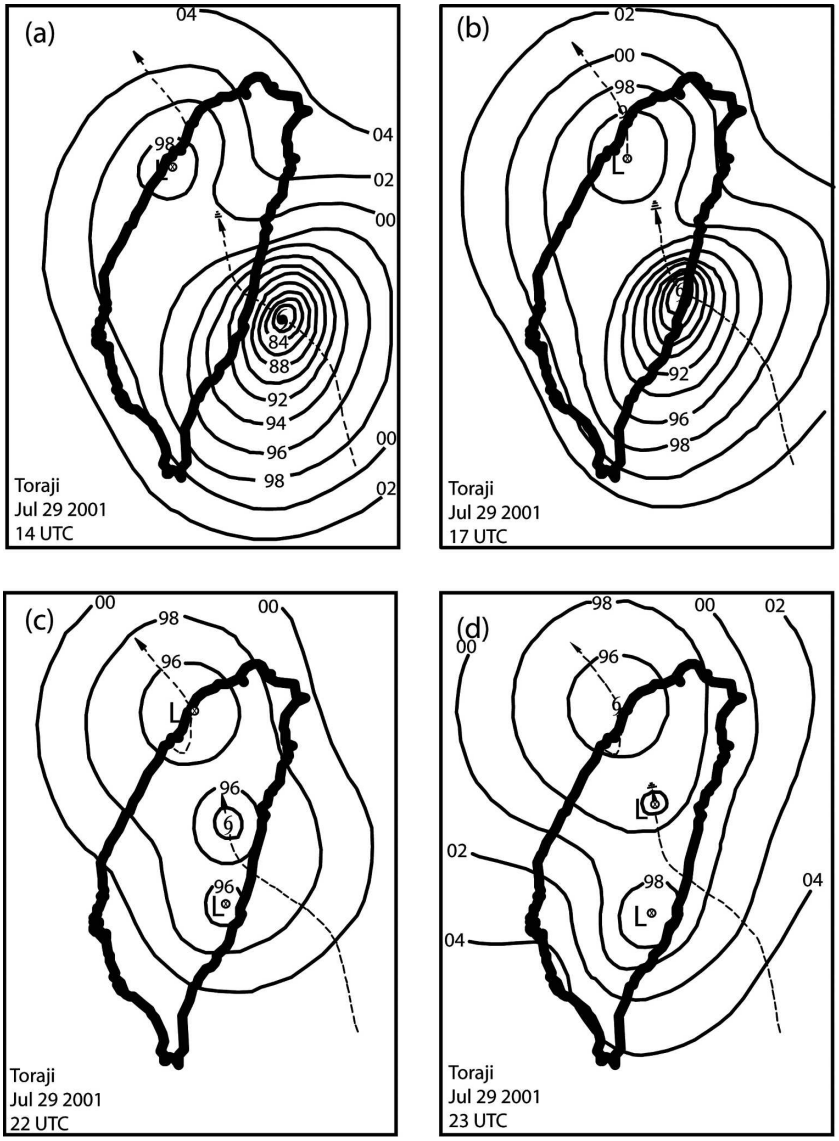

FIG. 7. Same as in Fig. 4, but for Toraji (in 2001).

4. Model simulation results and discussion

a. Simulation results of Bilis

As analyzed by CWB, the simulated Typhoon Bilis had a continuous track across CMR. Figure 9 shows the sea level pressure center and the 700, 500, and 300 mb geopotential height centers at 3-h intervals. Also shown are the observed 6-hourly positions of Bilis. Both of the tracks start at 0600 22 August 2000. The timing and track of the simulated typhoon was very close to observations. The simulated storm, like the observed storm, took an almost straight-line track over the CMR. By the time of landfall, the minimum pressure was near 930 mb, close to the observed pressure of around 920 mb as analyzed by the Japan Meteorological Agency (JMA).

The lower-, mid, and upper-level storm centers remain vertically stacked during and after the passage over Taiwan. One can also examine the vertical coherent structure of the storm via east–west vertical cross sections through the storm center of horizontal wind speed and PV (Figs. 10a–c). These east–west vertical cross sections were plotted at 3-h intervals while Bilis was crossing Taiwan. Figure 10a shows the vertical cross section through the center at 1200 UTC 22 August 2000 when it was still located east of Taiwan. The vertical structure of the storm is quite coherent with upper- and lower-level PV maxima and a shaft of weaker winds (the eye) extending the depth of the troposphere. At 1500 UTC 22 August 2000 (Fig. 10b), the center is located over the CMR. The eastern flank of PV remains

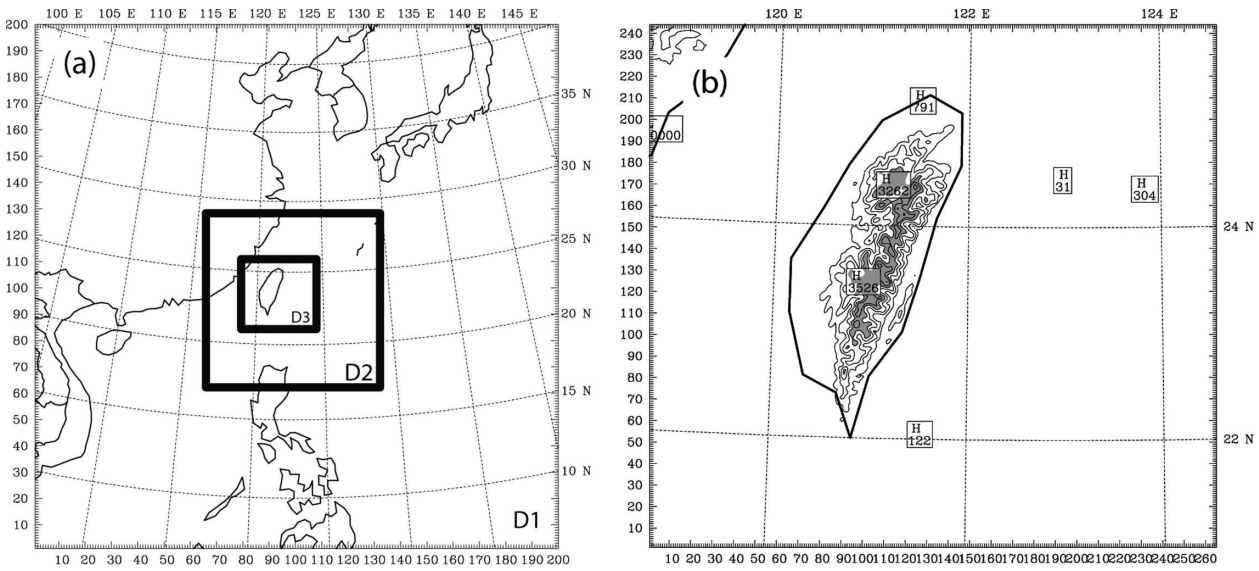

FIG. 8. (a) Domain configuration. Domain 1 (D1) has 200 × 200 grid points with 21-km grid resolution, domain 2 (D2) has 199 × 199 grid points with 7-km grid spacing, and domain 3 (D3) has 265 × 244 grid points with 2.3-km grid spacing. (b) Terrain (contour interval 500 m) used for D1. Shaded areas are above 2000 m.

vertically stacked, with the lower-level PV slightly weakened by the CMR.

One dramatic impact of the CMR on Bilis was the destruction of the western flank of the PV, which lost its vertical coherent structure. The upper-level PV was advected farther to the west, compared to the extrapolated position; the midlevel PV was weakened due to reduced low-level cyclonic circulation; and the low-level PV was severely weakened over the eastern slope due to orographic blocking. The asymmetry of the PV affected by the CMR at this time (Fig. 10b) appears to contribute to the disappearance of the eye on a satellite picture (not shown). Of note is a tongue of PV between 850 and 900 mb extending westward from the CMR. If the storm were weaker and/or slower, as in Typhoon Toraji, this tongue of PV would help spawn a new low-level center. At 1800 UTC (Fig. 10c), it is evident that this did not occur, as the lower- and upper-level PV maxima are once again coupled vertically. However, the eye is no longer an identifiable feature from satellite imagery. The CMR has weakened the system, with lower winds and amounts of PV being associated with the typhoon.

Shown in Figs. 10d–f are east–west cross sections of total water mixing ratio (q_w), potential temperature, and wind vectors at identical locations as in Figs. 10a–c. At 1200 UTC 22 August 2000 (Fig. 10d), the eyewall is clearly evident based on the shaded regions on either side of the center. These shaded regions correlate with higher PV regions (Fig. 10a). It is interesting to note that the total water mixing ratio shows a vertical upright structure, while the PV shows distinct outward tilt structure. Due to orographic forcing, they do not coincide 100%. The western eyewall convection is larger than the eastern eyewall convection due to orographic enhancement, leading to the slight distortion of the PV toward the west. At 1500 UTC (Fig. 10e), q_w has decreased around the center, due to the disruption of the circulation by the CMR. A corresponding decrease in PV is seen in Fig. 10b, due to less latent heat release and frictional effects. However, the upslope wind over western slope produced clouds and possibly rainfall, which helps increase the PV there (Fig. 10b). By 1800 UTC (Fig. 10f), q_w is the largest over the CMR, due to orographic forcing. The q_w on the west side of the circulation is significantly reduced.

Now we will examine the upper- and lower-level height centers in greater temporal detail. Figure 11 shows the pressure and vector wind fields at the surface, 700 and 300 mb at 1400–1700 UTC 22 August 2000. At 1400 UTC 22 August 2000, the center of Bilis is making landfall in southeast Taiwan. All of the surface pressure center, 700- and 300-mb geopotential height centers are located at the same location. An hour later (1500 UTC), the primary centers remain vertically stacked in southeast Taiwan. A weak center is located to the west of the CMR at the surface and 700 mb, likely from adiabatic warming as implied from the wind field depicted in Figs. 11–13. However, there is no evidence of a closed circulation developing in that area. At 1600 UTC, slight acceleration of the centers is evident. The surface and 700-mb centers are now located on the west

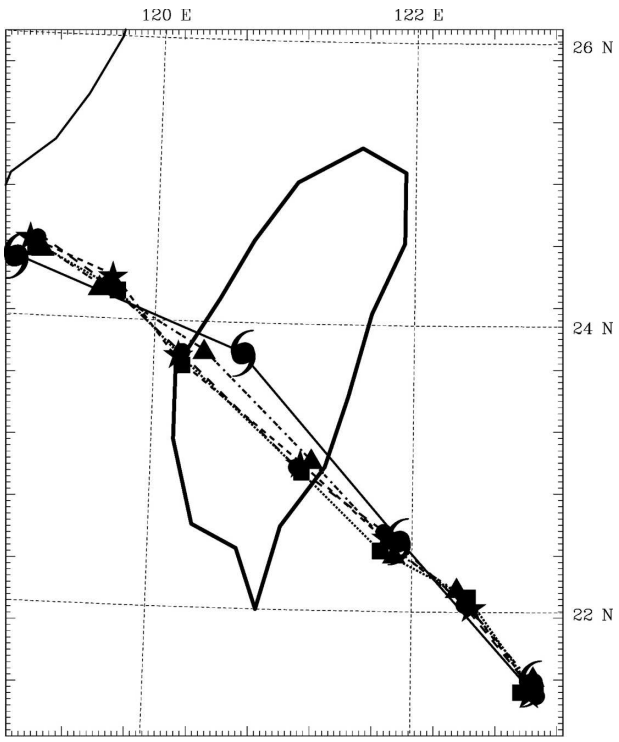

FIG. 9. Observed track (TC symbols) and center tracks from the model simulations for Bilis. The surface, 700-, 500-, and 300-mb centers are denoted by stars, squares, circles, and triangles, respectively. The observed track is every 6 h; model tracks are every 3 h. All of the tracks start at 0600 UTC 22 Aug 2000.

side of the CMR. The 500- (not shown) and 300-mb centers appear to be lagging slightly, still located over the CMR. By 1700 UTC, the centers are once again perfectly stacked in the vertical. It could be argued that there was a modification or redevelopment of the centers, slightly ahead of the original centers. However, the acceleration of the low-level center as it passed over the CMR is consistent with previous studies (Yeh and Elsberry 1993a,b, among others). Basically, the low centers crossed the mountain continuously without much disturbance.

Similar features can be found by looking at streamlines at the same levels. At 1400 and 1500 UTC 22 August 2000 (Fig. 12), the circulation centers of the original cyclone at different levels are collocated as Bilis makes landfall. There is no evidence of new circulation centers forming on the lee side of the CMR but the 700-mb center is elongated toward the west. By 1600 UTC, the surface and 700-mb centers are all located west of the CMR. The 300-mb circulation center, like the height center, is located over the CMR. Much like the geopotential height centers (not shown), low- and midlevel circulation centers accelerated toward the west as they crossed the CMR. By 1700 UTC, the circulation centers are vertically coupled and in the same location as the height centers.

One way to determine the mechanisms of track deflection and reformation is to look at the horizontal distribution of PV, especially at lower levels. The low-level PV can be generated and redistributed in a number of ways, two of which are from latent heat release and the turbulence associated with orographic blocking of the high terrain in the planetary boundary layer (Schär and Smith 1993a,b). Smith and Smith (1995) found that a vortex approaching an isolated mountain wraps a pair of vorticity banners into its circulation after it passes over the mountain. The potential vorticity production on the lee side as the cyclone approaches the mountain is explained by the transition from an irrotational flow regime to the regime of flow over a mountain with wakes through wave breaking. For a low Froude number, nonrotating, uniform flow, Schär and Durran (1997) found that the generation of leeside vorticity is due to the vertical tilting of baroclinically generated horizontal vorticity upstream at an earlier stage and due to potential vorticity generation at a later stage. Lin et al. (1999) showed that the increase in surface vorticity and the contraction of the cyclone scale on the lee side can be explained by the generation of new PV due to wave breaking associated with the severe downslope wind and hydraulic jump. The PV can also be generated from vorticity streamers through the gaps in the higher terrain of the CMR via stronger flow around the peaks of the CMR or via increased gap flow in the Taiwan Strait (Schär and Smith 1993a,b).

For Bilis, the adiabatic warming was especially intense. Figure 13 shows the 850-mb geopotential height and temperature fields at 1400–1700 UTC 22 August 2000. Downstream of the northern CMR, the air is 6–8 K warmer than on the upstream side. This warming has caused a distortion in the height field, with lower heights in the same area of adiabatic warming. As the center crosses the CMR, the center takes a cyclonic turning and produces adiabatic warming on the west side (i.e., lee side of the outer circulation). The resultant height drop in the area of the adiabatic warming appears to be partially responsible for the northward jog of the center as it crossed the CMR.

Further insight can be gathered by looking at backward trajectories from the time when the circulation became well established on the west side of the CMR. The backward trajectories are calculated from the path of a parcel based on the model-derived winds. The result represents the approximate path a parcel took to get to its final destination. Backward parcel trajectories were examined at 0.9, 0.8, 0.7, and 0.6 sigma levels, going backward 6 h from 1700 UTC 22 August 2000.

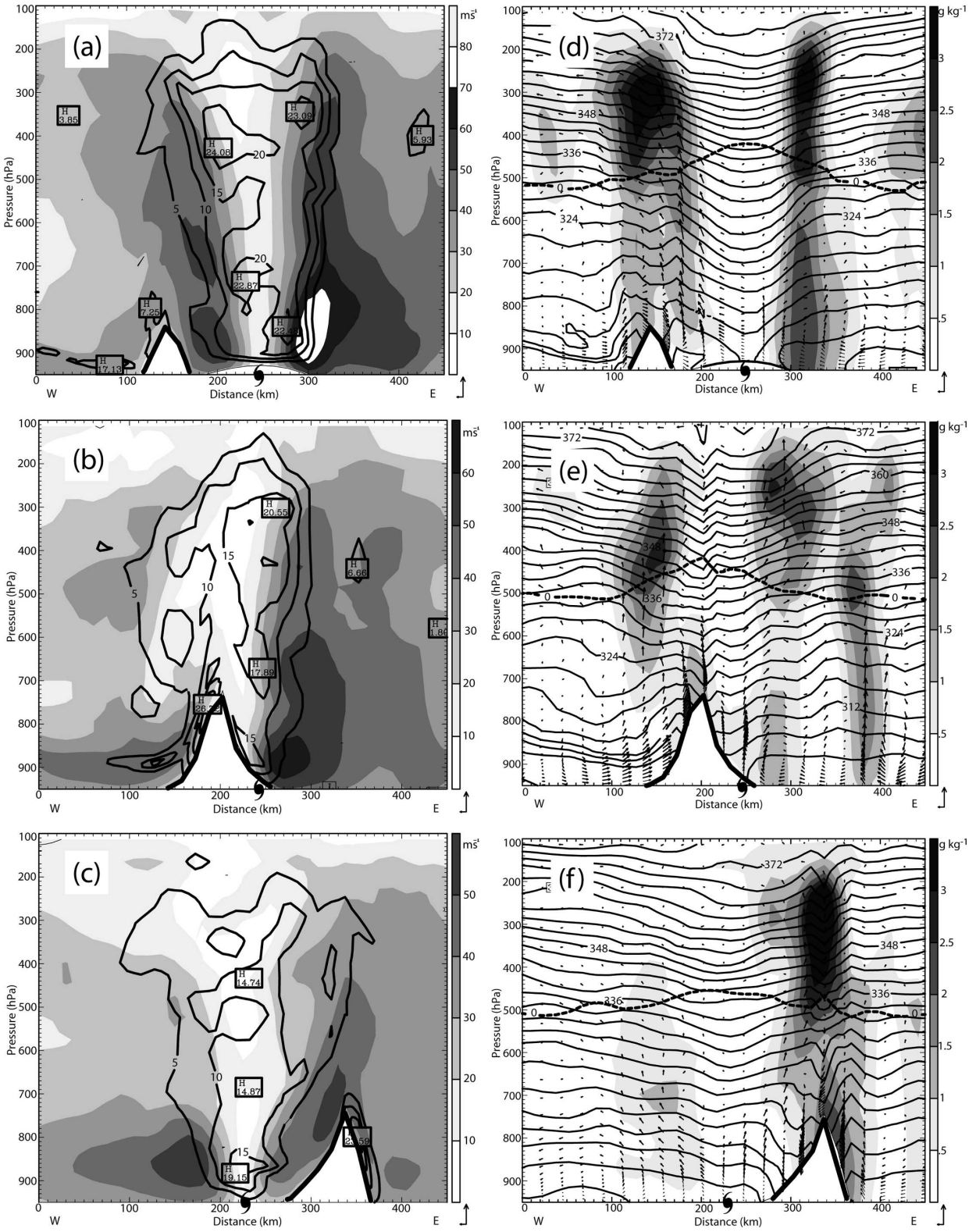

FIG. 10. East–west cross sections of horizontal wind speed (shaded) and PV (contours in PVU; 1 PVU = 10^{-6} m^2 s^{-1} K kg^{-1}) through the primary storm center for Typhoon Bilis (in 2000) at (a) 1200, (b) 1500, and (c) 1800 UTC 22 Aug 2000. (d)–(f) Same as (a)–(c) but for the total water mixing ratio (q_w shaded, in g kg^{-1}), θ (K, thin lines), freezing level (thick dashed line), and wind vectors for Typhoon Bilis. Closed TC symbols denote the location of the typhoon center.

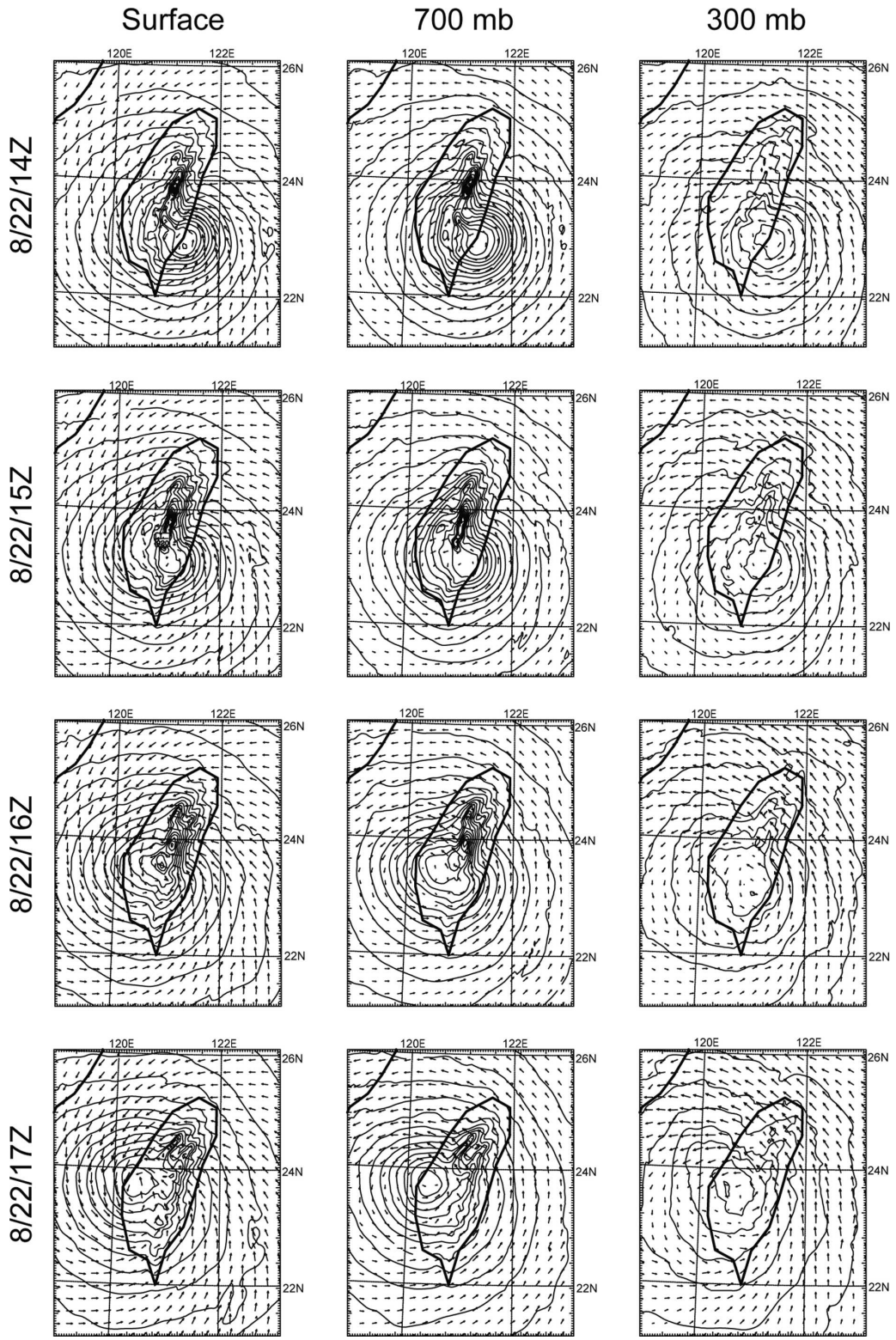

FIG. 11. Simulated sea level pressure and wind vectors for Typhoon Bilis at (left column) surface, (middle column) 700 mb, and (right column) 300 mb for (first row) 1400, (second row) 1500, (third row) 1600, and (fourth row) 1700 UTC 22 Aug 2000. Contour intervals at surface, 700 hPa, and 300 hPa are 4 hPa, 30 m, and 30 m, respectively.

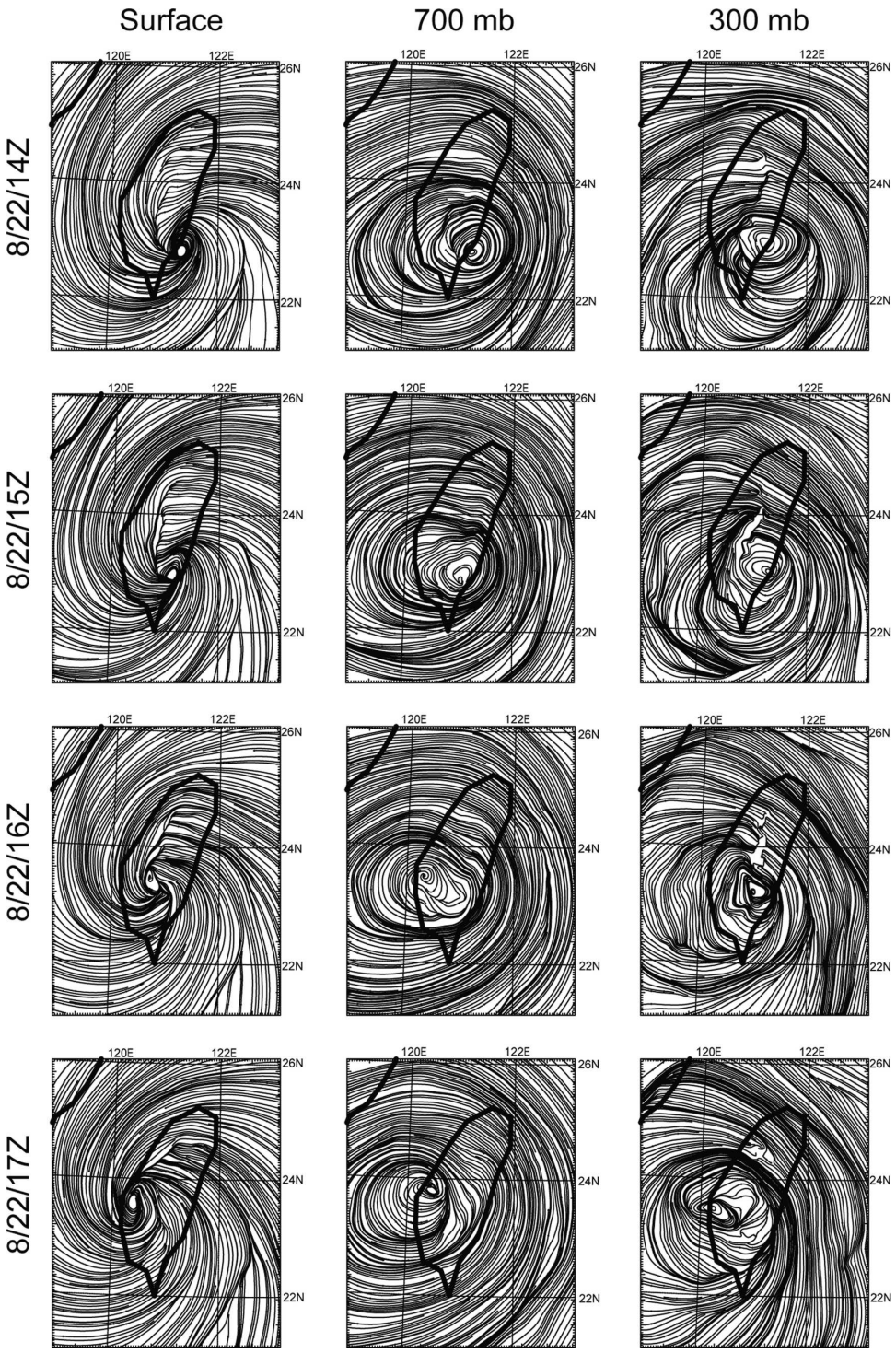

FIG. 12. Same as in Fig. 11, but for streamlines.

Parcels at the lowest levels ($\sigma = 0.9$) to the south of the circulation center (parcels 3 and 4, Fig. 14a) went around the north side of the CMR, while parcels on the north side of the circulation center (parcels 1 and 2) traveled over the CMR. At $\sigma = 0.8$ and 0.7 (Figs. 14b,c), all parcels traveled over the central CMR. At $\sigma = 0.6$ (Fig. 14d), the southern three parcels originated from the east of Taiwan, and traveled over the CMR.

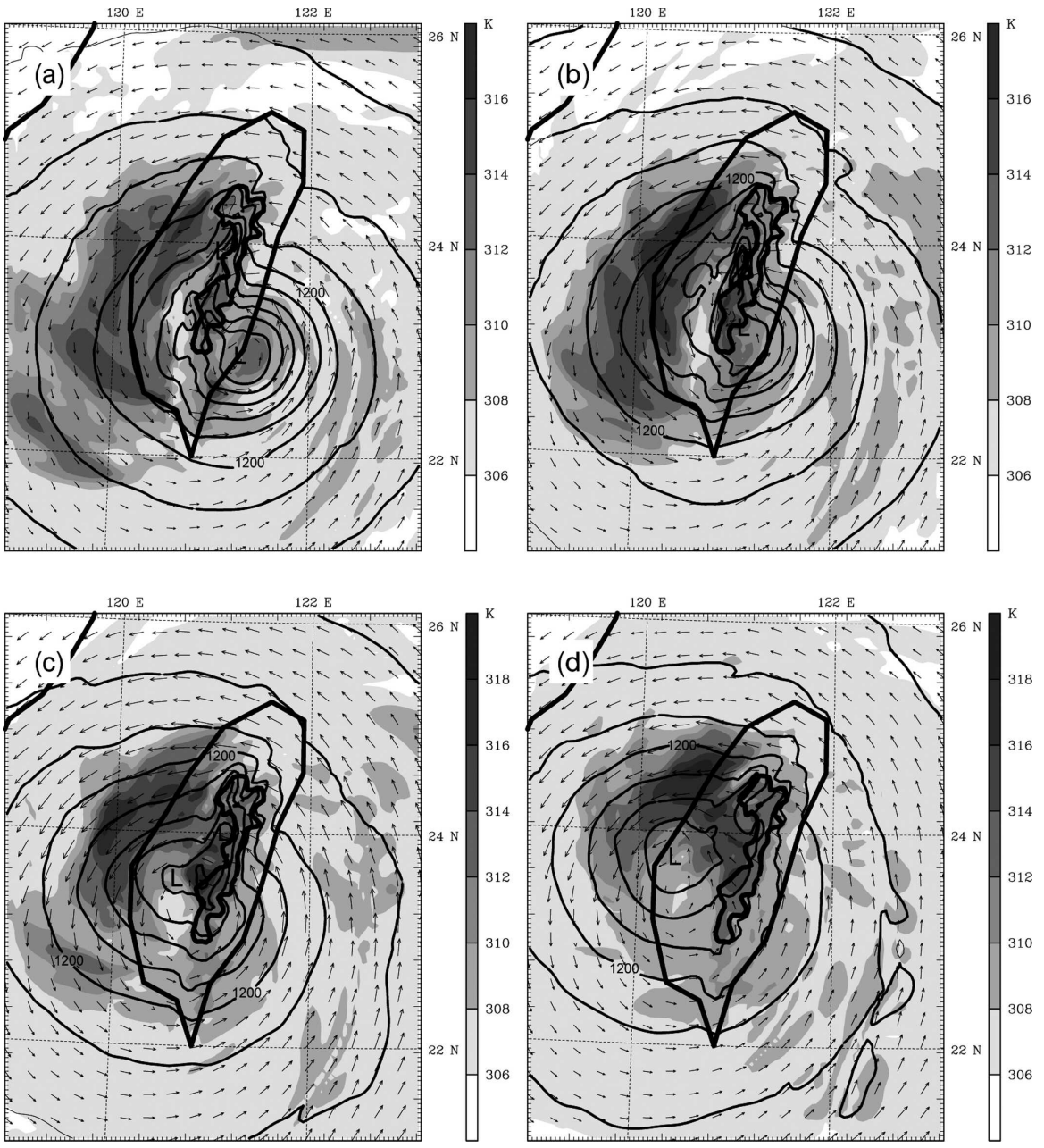

FIG. 13. Simulated 850-mb height (contours), temperature (shaded, K), and wind vector field for Typhoon Bilis at (a) 1400, (b) 1500, (c) 1600, and (d) 1700 UTC 22 Aug 2000. The height contour interval is 60 m.

The northern most parcel traveled around the northern portion of the CMR, then climbed up the east slope of the CMR before turning cyclonically around the circulation center. Parcel 2 exhibits a troichoidal motion throughout its history, indicating that the circulation center maintained itself (i.e., it was continuous) at this level. All parcels at each level originated from near the surface.

Figure 15 shows the 850-mb geopotential height and PV for the hours when Bilis was crossing the CMR. At 1400 UTC 22 August 2000 the center is making landfall, and the high PV near the center is easy to identify (Fig. 15a). Areas of negative PV are located on the eastern slope of the CMR, due to turbulence produced by strong blocking against the CMR in the planetary boundary layer. On the western slope of the CMR, cyclonic vorticity associated with vorticity stretching over the lee (western) slope, and downstream advection of the latent heat released over upslope (Lin et al. 1999)

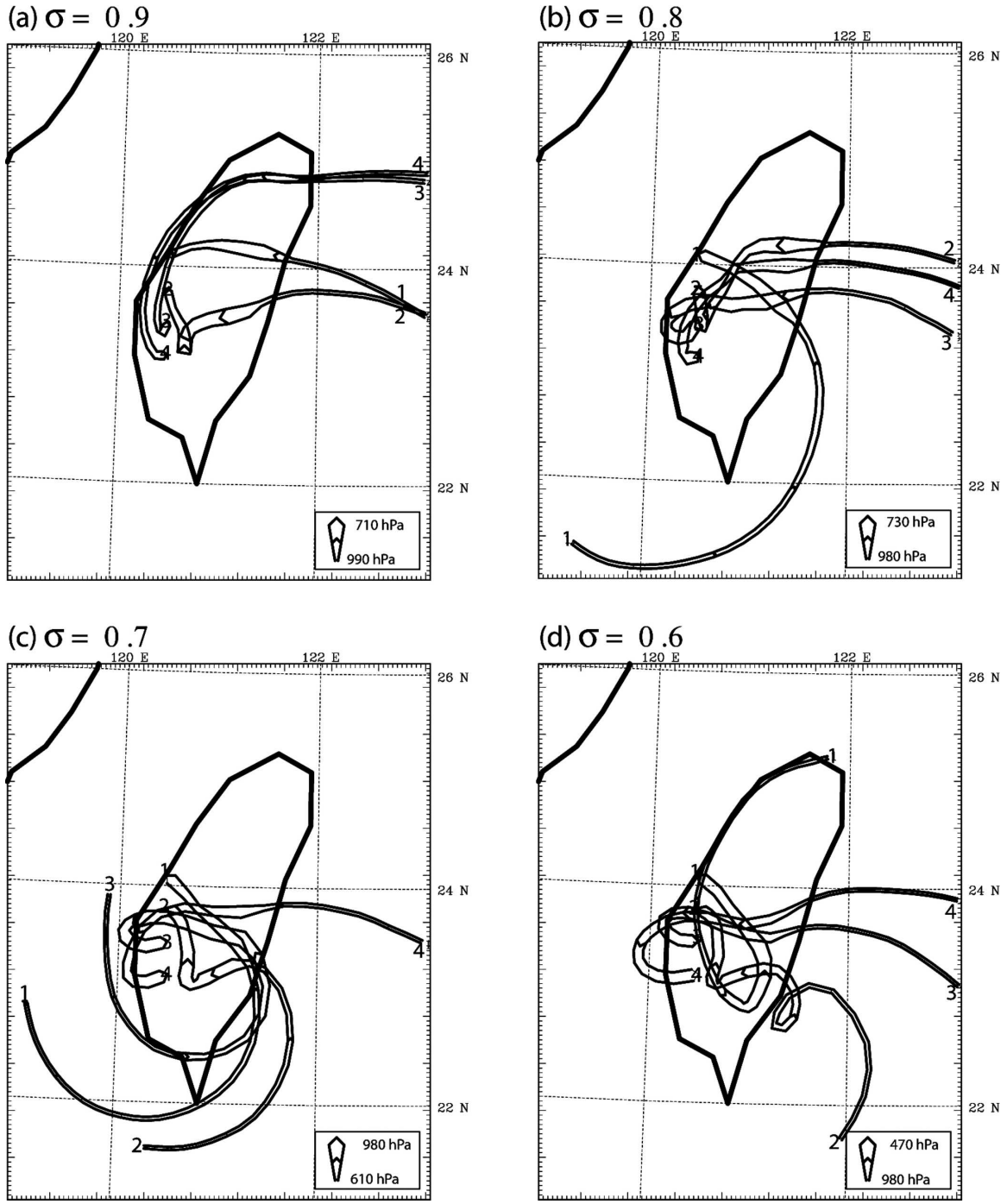

FIG. 14. Simulated backward trajectories starting from 1700 UTC 22 Aug 2000 for Bilis. The heights are σ = (a) 0.9, (b) 0.8, (c) 0.7, and (d) 0.6. Narrower (wider) ribbons denote air parcel at lower (higher) levels.

created a broad area of positive PV. Flow through the mountain gaps between mountain peaks creates alternate areas of positive and negative PV banners downstream. An impressive PV banner extended from the north of Taiwan, as the air went around the northern portion of the CMR. The large PV streamer ultimately becomes wrapped up into the center once it passes over the CMR (Fig. 15d).

b. Simulation results of Toraji

The forward speed of Toraji was slower and the intensity was weaker than that of Bilis, allowing a more

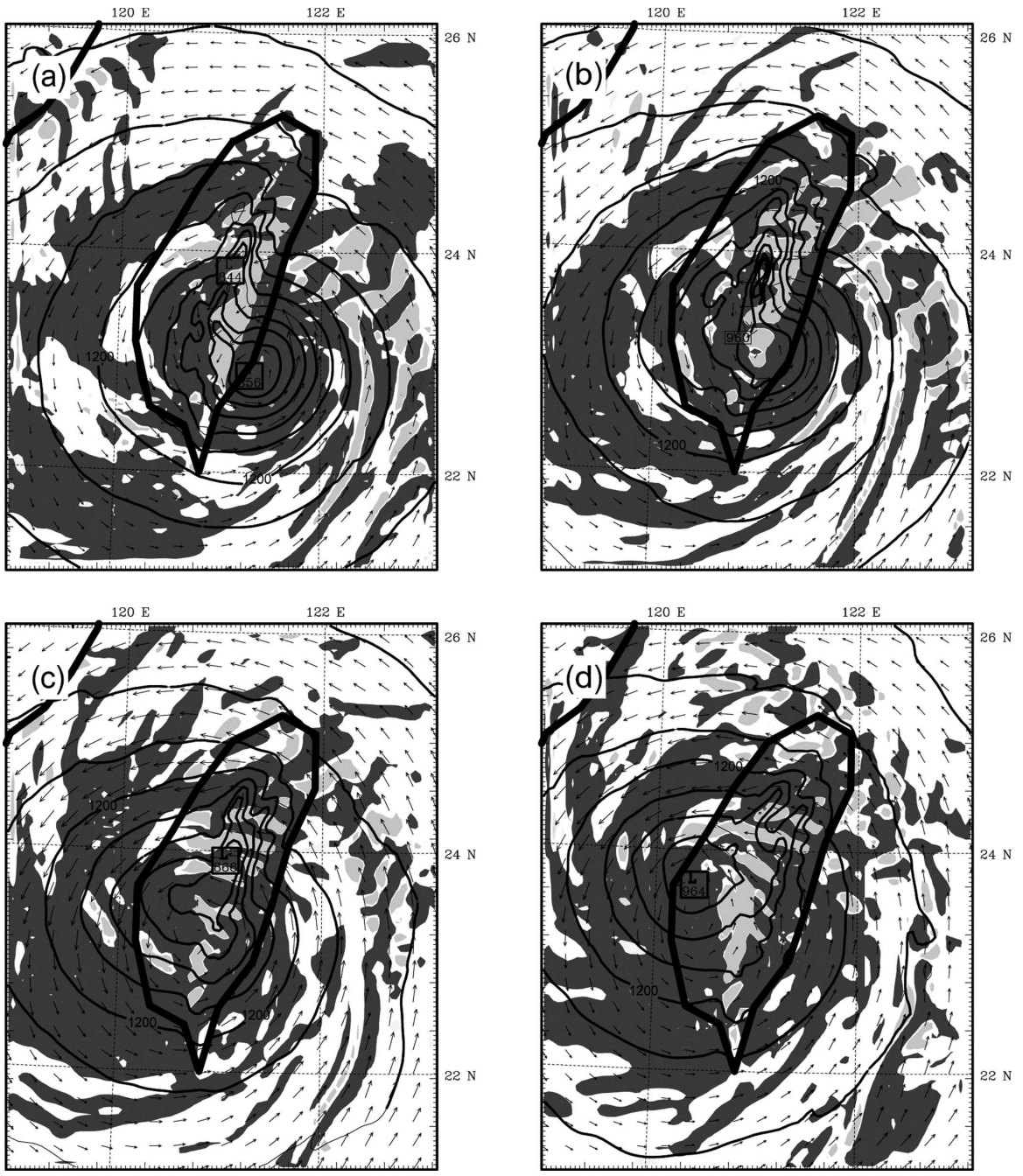

FIG. 15. Simulated 850-mb geopotential height, PV, and vector wind fields for Bilis at (a) 1400, (b) 1500, (c) 1600, and (d) 1700 UTC 22 Aug 2000. Areas of PV > 1 PVU are denoted by dark gray, while areas of PV < -1 PVU are denoted by light gray. (1 PVU $= 10^{-6}$ m^2 s^{-1} K kg^{-1}.)

complicated interaction with the CMR. Unlike Bilis, the storm structure did not remain vertically coherent on its path over the CMR, resulting in a discontinuous track. The simulated Toraji behaved similarly to the real Toraji. Figure 16 shows the observed Toraji track (every 6 h) and the model simulated sea level pressure center, and the 700-, 500-, and 300-mb geopotential height centers at 3-h intervals. The centers remain vertically coherent until making landfall in central Taiwan and new low-level centers form on the west side of the CMR, to the south of the extrapolated path. This secondary center soon becomes the dominant center, while the old low-level center weakens and dissipates. The upper-level centers dissipate as the old primary

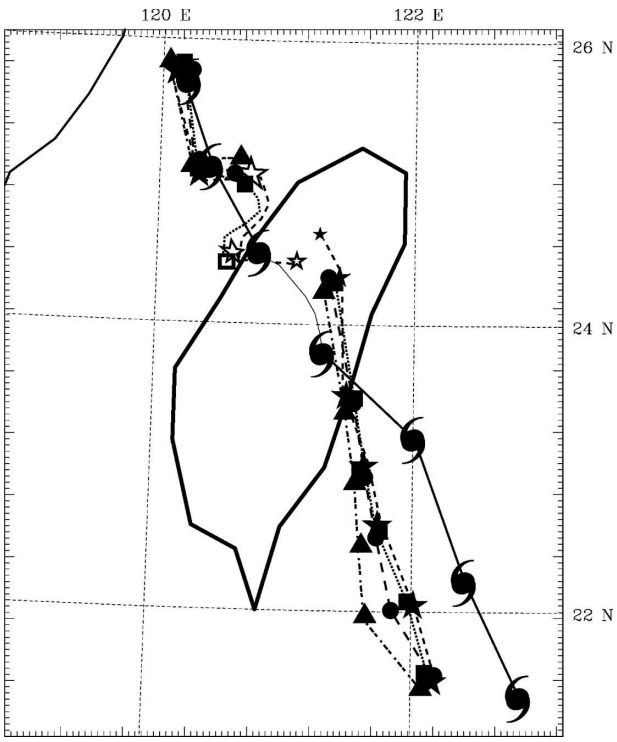

FIG. 16. Observed track (TC symbols) and center tracks from the model simulations for Toraji. The surface, 700-, 500-, and 300-mb centers are denoted by stars, squares, circles, and triangles, respectively. The observed track is every 6 h, model tracks are every 3 h; both start at 0600 UTC 29 Jul 2001. Outlined symbols indicate two centers coexisting simultaneously.

low-level centers die, and reform over the new low-level center. This will be shown later.

The vertical cross sections also portray the center reformation on the lee side. At 1200 UTC 29 July 2001, the storm has robust vertical orientation, with the upper-level center located over the lower-level PV maximum (Fig. 17a). During the next two 3-h increments (left panels of Figs. 17b,c), the center retains its vertical structure as it comes ashore. During this period, a new secondary low-level center is generated in the lee of the CMR. The right panels of Figs. 17b,c are cross sections through the new secondary center. A PV maximum at the low levels was present to the west of the CMR, a product of adiabatic warming from the downslope flow and the generation of a secondary vortex, as the outer circulation of Toraji went around the northern CMR. In addition, an area of lighter winds was present just above the low-level PV, with stronger winds to the west in the Taiwan Strait. By 2100 UTC 29 July 2001 (Fig. 17d), a low-level PV maximum and low-level circulation became established west of the CMR, while the upper-level PV maximum remained over the CMR. At 0000 UTC 30 July 2001 (Fig. 17e), the new center has extended in the vertical, coupled with the remnant higher-level PV to the east being all that remains of the old upper-level center. Note that the cross section at this time is to the north of Taiwan. Thus, for a weaker typhoon, the low-level PV is destroyed by the interaction with the CMR. When the low-level support vanishes, the mid- and upper-level PV gradually weakens. As the outer circulation impinges on the CMR, a new low-level PV center forms on the lee side, ultimately takes over as the new center, and couples with the remnant of the upper-level PV.

Figure 18 shows total water mixing ratio q_w, potential temperature, and wind vector fields on the same cross sections in Fig. 17. When the center is offshore (Fig. 18a), the distribution of q_w is asymmetric with greater concentrations above the CMR, corresponding with the tilt of the PV toward the west. By the end of the next 3 h (Fig. 18b), the greatest q_w are in the eastern eyewall, with lesser concentrations over the CMR. The convection on the western eyewall has been disrupted significantly, allowing the greatest latent heat release, and resulting PV, to be concentrated on the eastern eyewall. At the time of landfall (Fig. 18c), higher q_w was located almost entirely over the CMR. At 2100 UTC 29 July 2001 (Fig. 18d), concentrations of q_w remain greatest over and above the CMR, keeping the highest PV in that area. Little if any concentrations of q_w are associated with the new low-level center to the west of the CMR (right panel of Fig. 18d). By 0000 UTC 30 July 2001 (Fig. 18e), the highest q_w remained in the layer of 300–500 mb, supporting an eastward extension of PV in that layer. Lower concentrations of q_w are now associated with the secondary center, helping to extend the PV maximum to greater altitudes due to latent heating.

To investigate the reformation mechanism of the secondary low and vortex of Toraji, we take a closer look at the evolution of the height centers as the storm crossed the CMR. At 1700 UTC 29 July 2001 (Fig. 19), Toraji makes landfall in central Taiwan. The lower- and upper-level centers are still collocated at this time. However, a new surface low has formed to the west of the CMR. Note that the surface flow started to circle around the secondary low on the lee side due to more flow going around the northern tip of the CMR, but the wind blew straight through over the surface secondary vortex. This agrees with the mechanism proposed by LCHH that the secondary vortex on the lee side is mainly produced by vorticity advection, similar to idealized simulations (LCHH). At 1900 UTC, the primary centers still have good vertical coherence, now over the CMR. The secondary low has strengthened, now having a weak circulation at the surface and a weak wake vor-

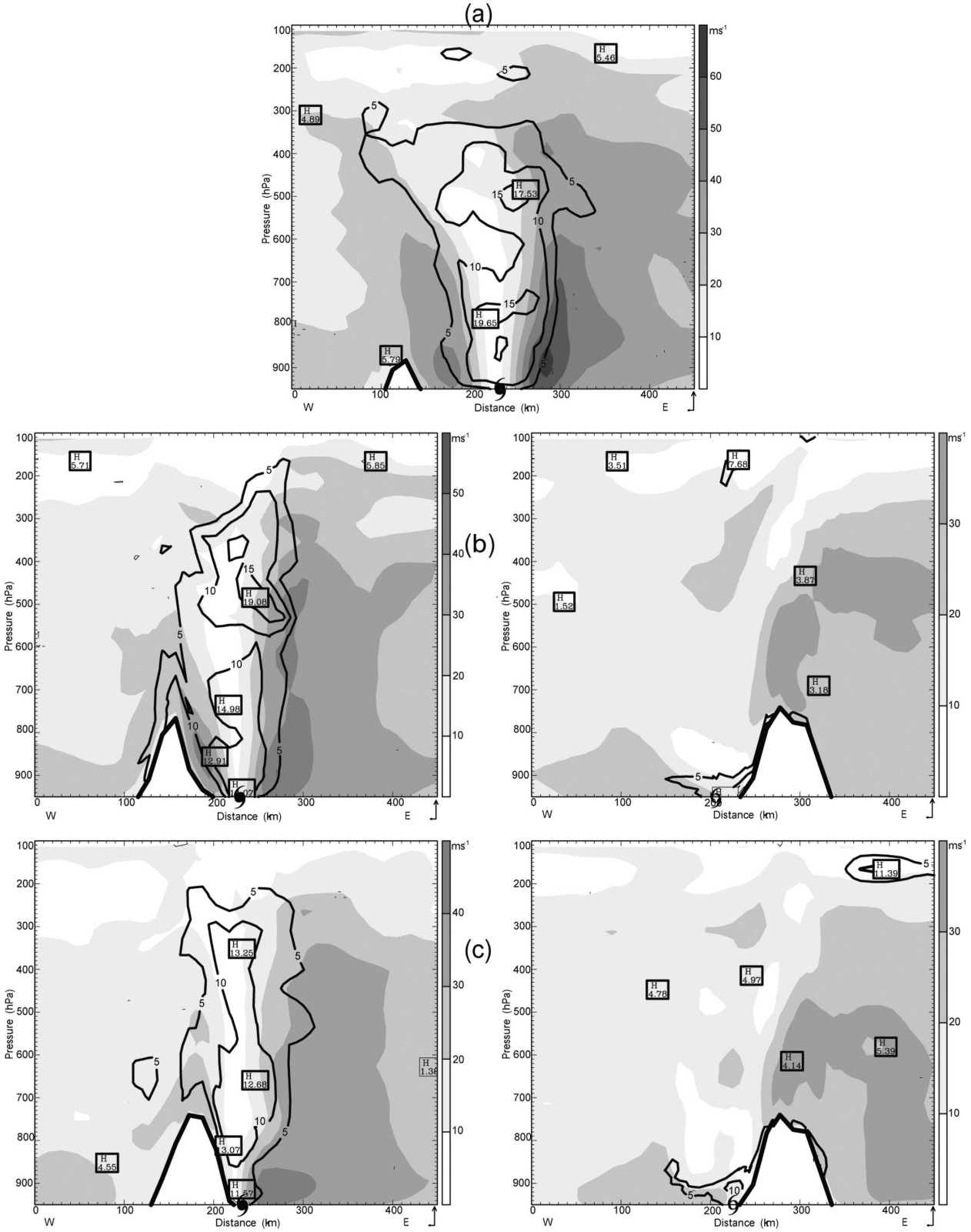

FIG. 17. East–west cross sections through the (a), (e), (left) primary and (right) secondary centers of horizontal wind speed (shaded) and PV (contours, PVU) for Typhoon Toraji at (a) 1200, (b) 1500, (c) 1800, (d) 2100 UTC 29 Jul, and (e) 0000 UTC 30 Jul 2001. Note that in (b)–(d), the secondary center at earlier time develops into (e) the primary center at 0000 UTC 30 Jul 2001. Closed and open typhoon symbols denote the locations of the original low center and the secondary new low center.

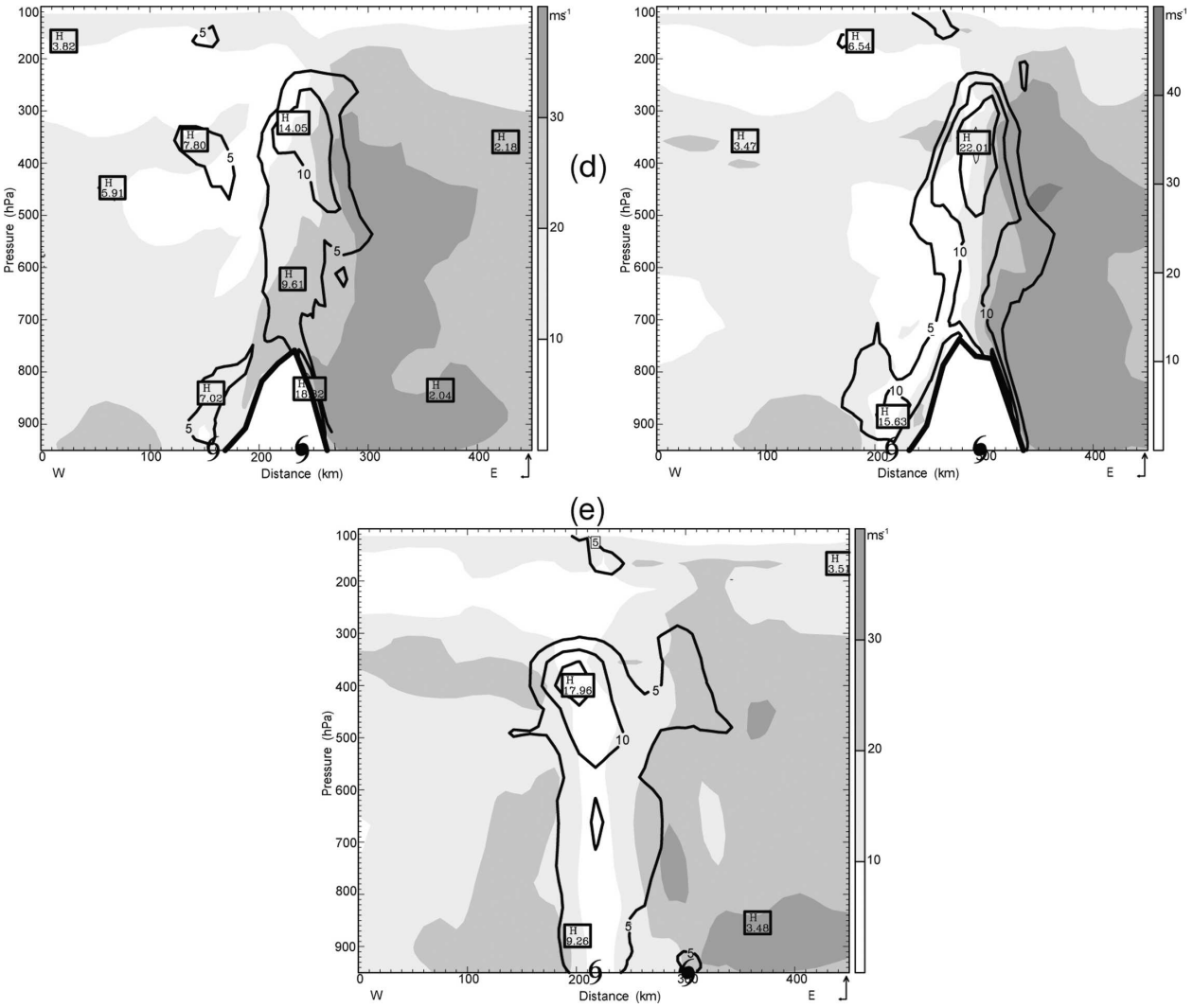

FIG. 17. (*Continued*)

tex at 700 mb. The upper-level lows weakened significantly at this time. At 2100 UTC, the secondary circulation has strengthened further, while the primary center continues to weaken. The secondary center now extends to 500 mb (not shown). By 2300 UTC, the surface secondary center has taken over the original cyclone.

The reformation process shows up even more clearly in the streamline plots (Fig. 20). At 1700 UTC 29 July 2001, the streamline centers were all just off the central-east coast of Taiwan. At the surface, there is significant curvature to the streamlines on the west side of the CMR where the secondary center forms. At 1900 UTC, the primary streamline centers have just come onshore. On the lee side a closed center at the surface has just formed, while the circulation at 700 mb (and to a lesser extent the 500-mb center) has significantly elongated to the west, toward, and over the new circulation. At 2100 UTC, the secondary streamline center has become dominant at the surface and 700 mb. At 500 mb (not shown), the center is roughly halfway between the primary and secondary centers. The 300-mb center remains over the CMR with the primary center with little reflection of the secondary center at that level. By 2300 UTC, the new center becomes coupled with upper-level centers.

For Toraji, the area of downslope winds, as depicted by the 850-mb temperature field (Fig. 21), was not as extensive as for Bilis due to the weaker winds associated with it. At 1700 UTC 29 July 2001, Toraji was making landfall. A large area of adiabatic warming was present off the northwest coast with a smaller area of adiabatic warming located at the southeastern corner of the CMR to the south of the center. Over time, the area

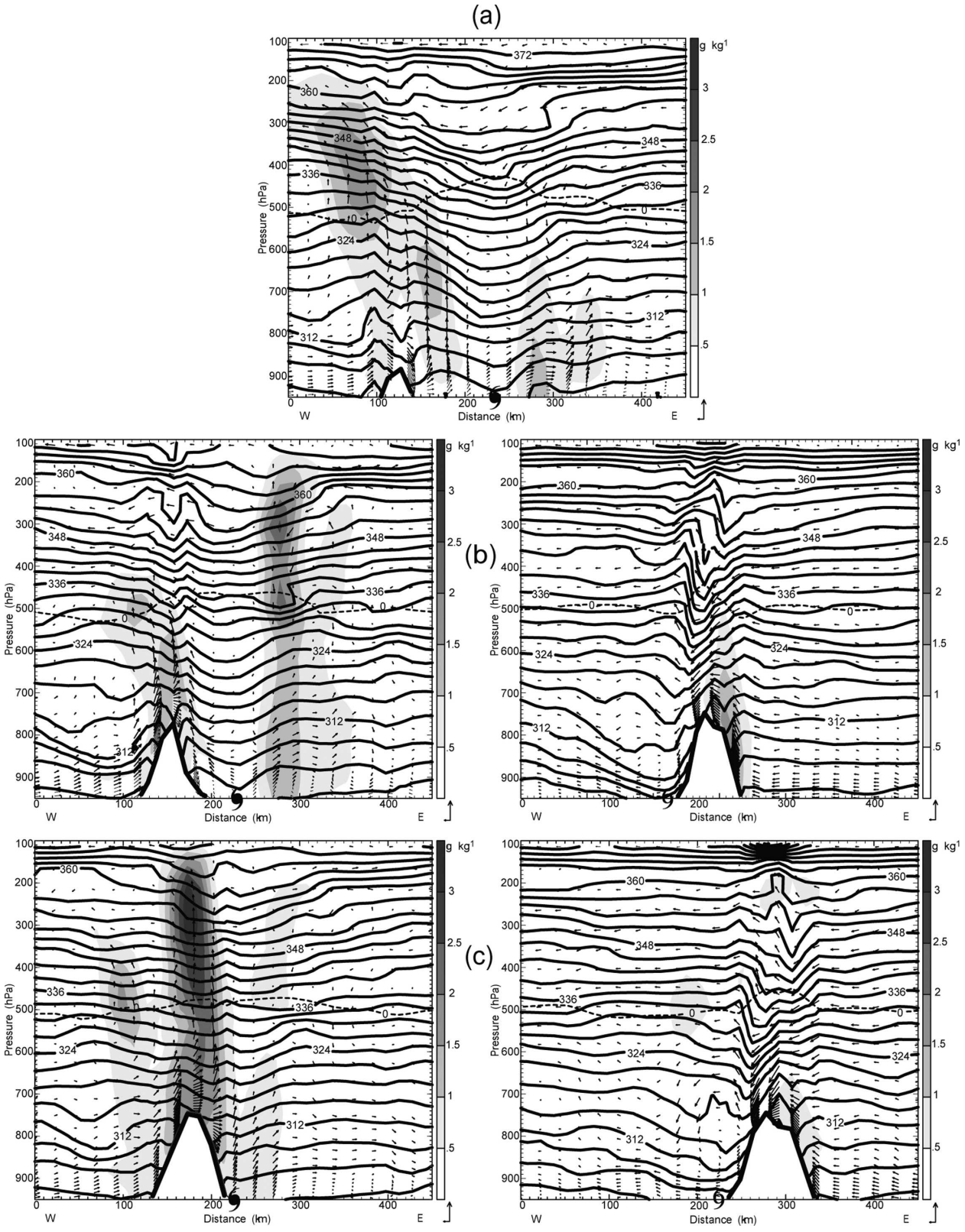

FIG. 18. Same as in Fig. 17 but for total water mixing ratio (q_w, shaded, in g kg^{-1}), potential temperature (K, thin lines), freezing level (thick dashed line), and wind vectors. Closed and open typhoon symbols denote the locations of the original low center and the secondary new low center.

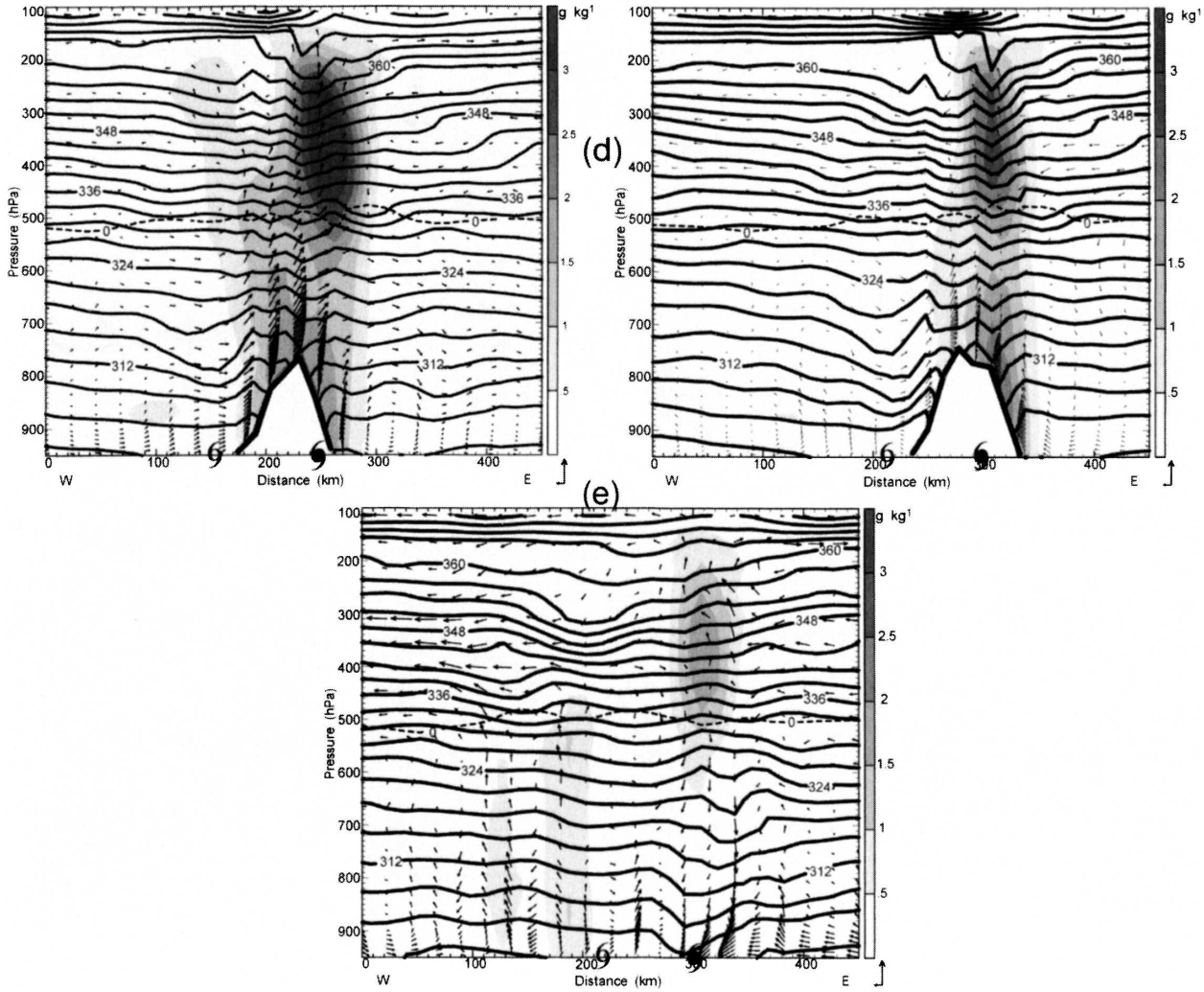

FIG. 18. (*Continued*)

to the northwest became the focus for the formation and development of the secondary circulation center.

The parcels for Toraji behaved in a different fashion. Figure 22 shows 6-h backward trajectories for parcels ending at 2100 UTC 29 July 2001. At lower levels (Figs. 22a,b), the parcels tended to go around the northern portion of the CMR. Parcels 3 and 4 traveled in a slight cyclonic path before ascending over the CMR, around the circulation of the primary center. Once over the CMR, the trajectories curved sharply toward the secondary center. Parcel 2 had the shortest path of all, as it was very near the secondary center after crossing the CMR. Parcel 1 initially orbited the primary center but was quickly drawn into the secondary center once the primary center made landfall. At the midlevels (Figs. 22c,d) the parcels initially wrapped around the primary circulation but then became entrained into the secondary circulation. As in Bilis, the parcels originated at low levels. Once the parcels crossed the CMR, the convection released latent heat, raising the potential temperature. On the lee side of the CMR, the parcels remained at a higher level due to their higher potential temperature.

Similar to Bilis, a banner of PV at 850 mb was present extending from the north tip of the CMR as Toraji made landfall at 1700 UTC 29 July 2001 (Fig. 23a). The primary difference is that the PV banner extended more northwestward than for Bilis. The PV banner was also located closer to the area of greatest adiabatic warming. By 2100 UTC (Fig. 23c), the PV banner had wrapped into the secondary circulation center and by 2300 UTC (Fig. 23d) it had become the primary center. The combination of adiabatic warming and the vorticity banner appear to have generated a PV maximum on the lee side of the northern CMR, helping to generate the secondary center, which ultimately became dominant.

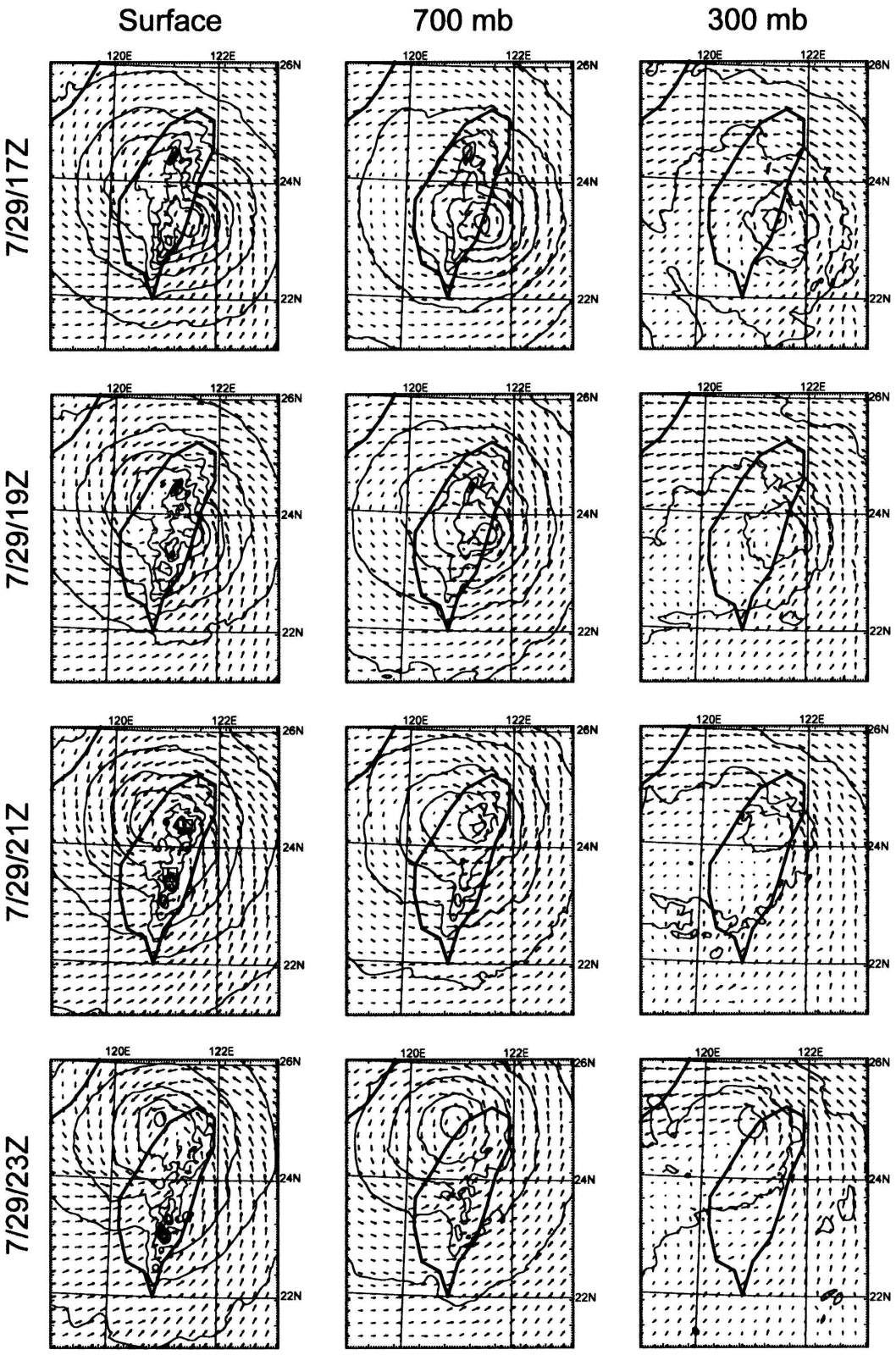

FIG. 19. Simulated sea level pressure and wind vectors for Typhoon Toraji at (left column) surface, (middle column 700 mb, and (right column) 300 mb for (first row) 1700, (second row) 1900, (third row) 2100, and (fourth row) 2300 UTC 29 Jul 2001. Contour intervals at surface, 700 hPa, and 300 hPa are 4 hPa, 30 m, and 30 m, respectively.

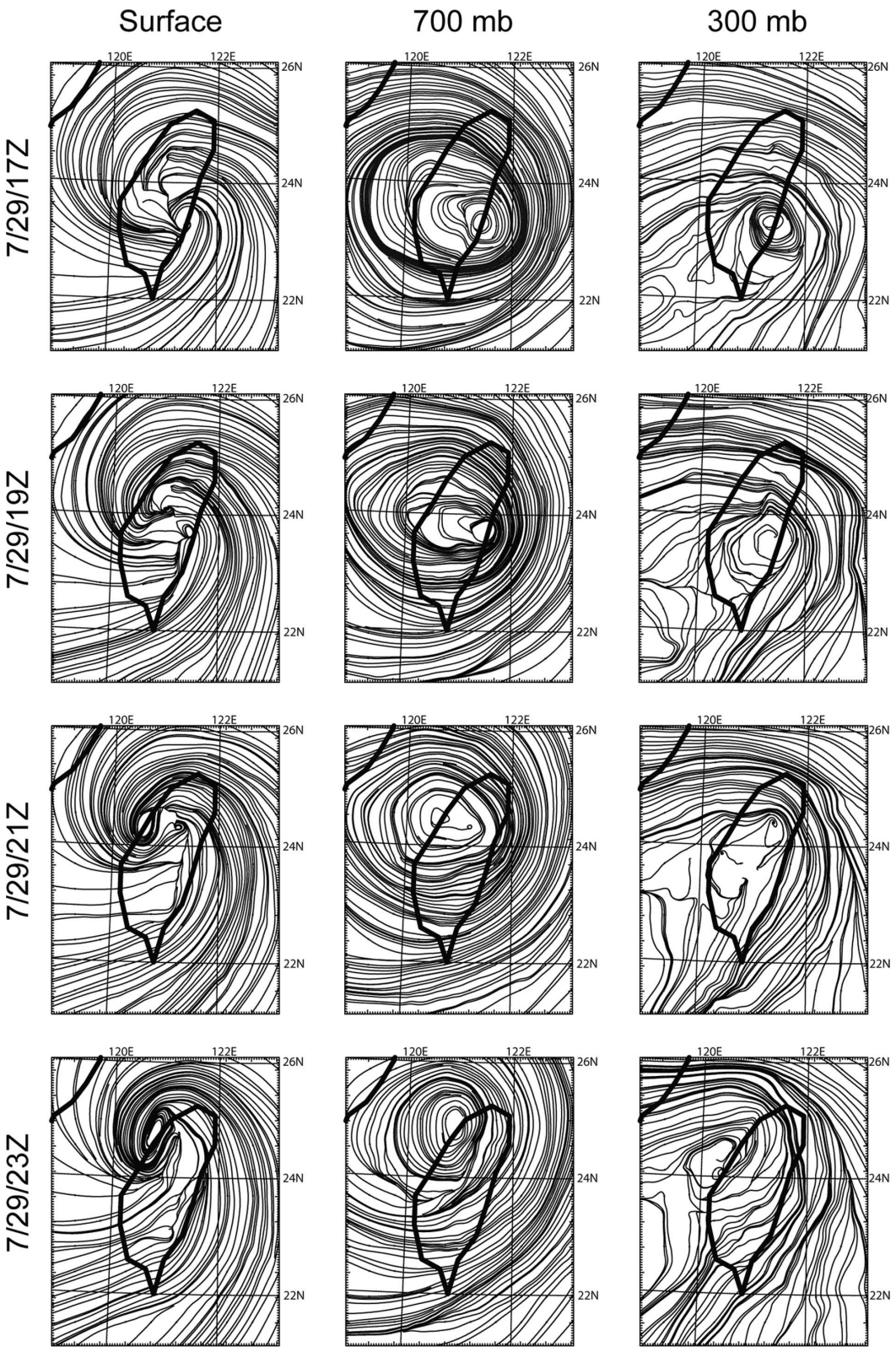

FIG. 20. Same as in Fig. 19, but for streamlines.

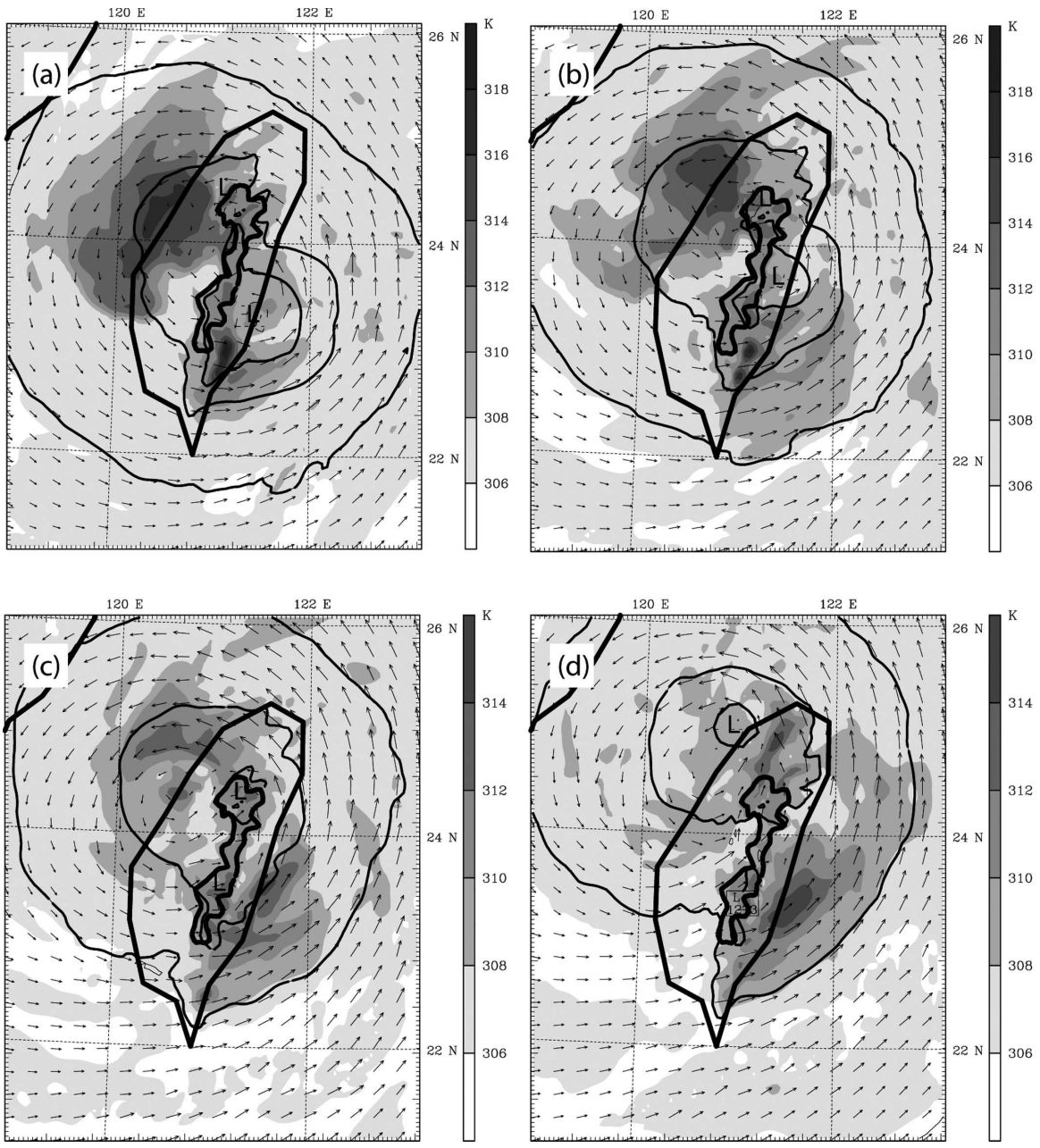

FIG. 21. The 850-mb height (contours), temperature (shaded, K), and wind vector fields for Typhoon Toraji at (a) 1700, (b) 1900, (c) 2100, and (d) 2300 UTC 29 Jul 2001.

5. Mechanisms of track continuity and deflection

a. A review of control parameters for track continuity and deflection

Based on idealized simulations of westward-moving cyclones over a north–south-oriented mesoscale mountain range, LCHH found that the cyclone track becomes discontinuous (continuous) and the cyclone experiences more (less) deflection with a combination of small (large) values of V_{max}/Nh, U/Nh, R/L_y, U/fL_x, and V_{max}/fR, and a large (small) value of h/L_x, where V_{max} is the maximum tangential wind, N is the Brunt–Väisälä frequency, h is the mountain height, U is the basic wind speed, R is the radius of V_{max}, f is the Coriolis parameter, and L_x and L_y are the horizontal scales of the mountain in x and y directions, respectively. The parameter U/Nh can be viewed as the Froude number of the basic flow. For TCs, U may be taken as the forward

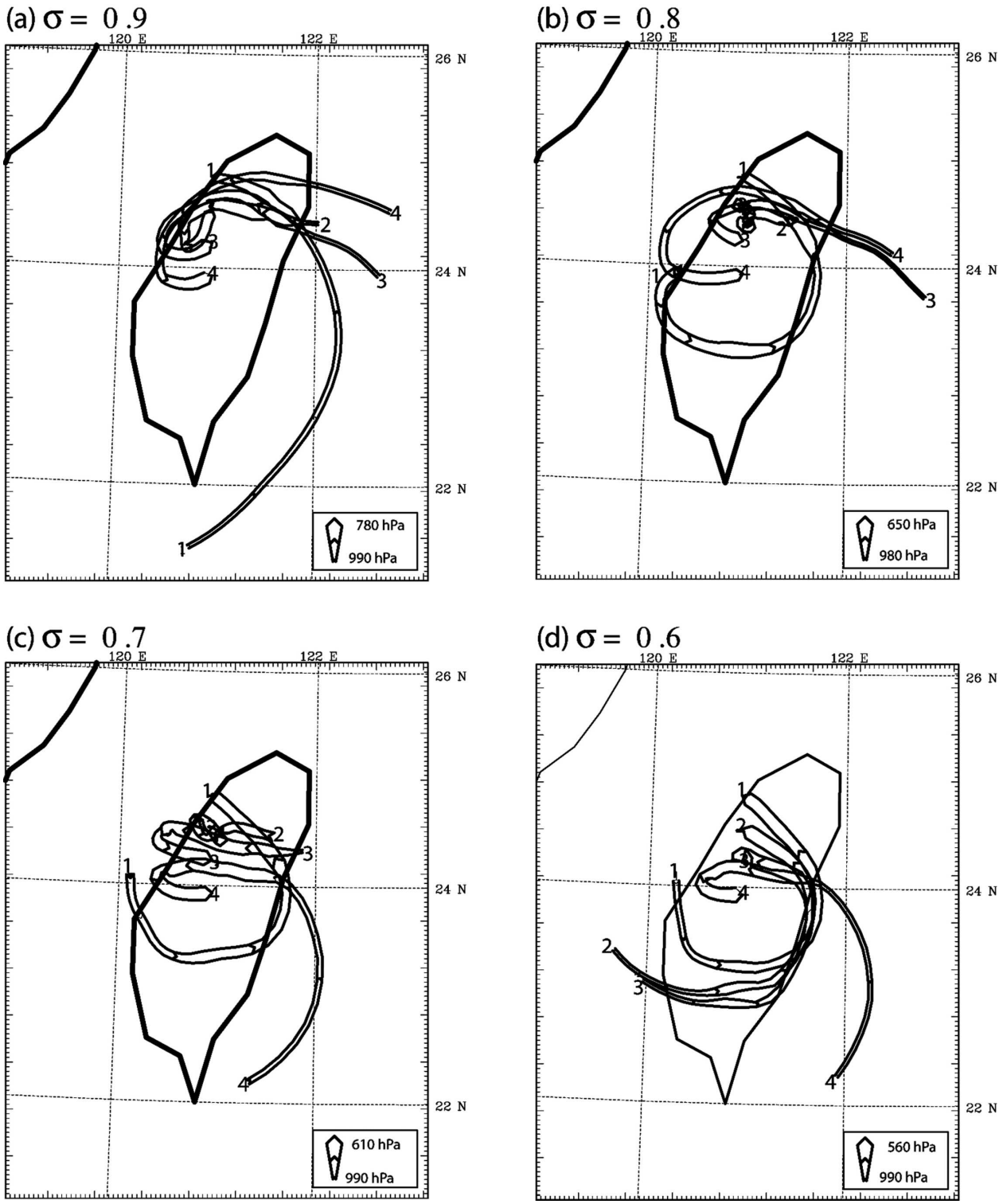

FIG. 22. Backward trajectories from 2100 UTC 29 Jul 2001 for Typhoon Toraji at σ = (a) 0.9, (b) 0.8, (c) 0.7, and (d) 0.6. Thinner ribbons are lower; wider ribbons are higher.

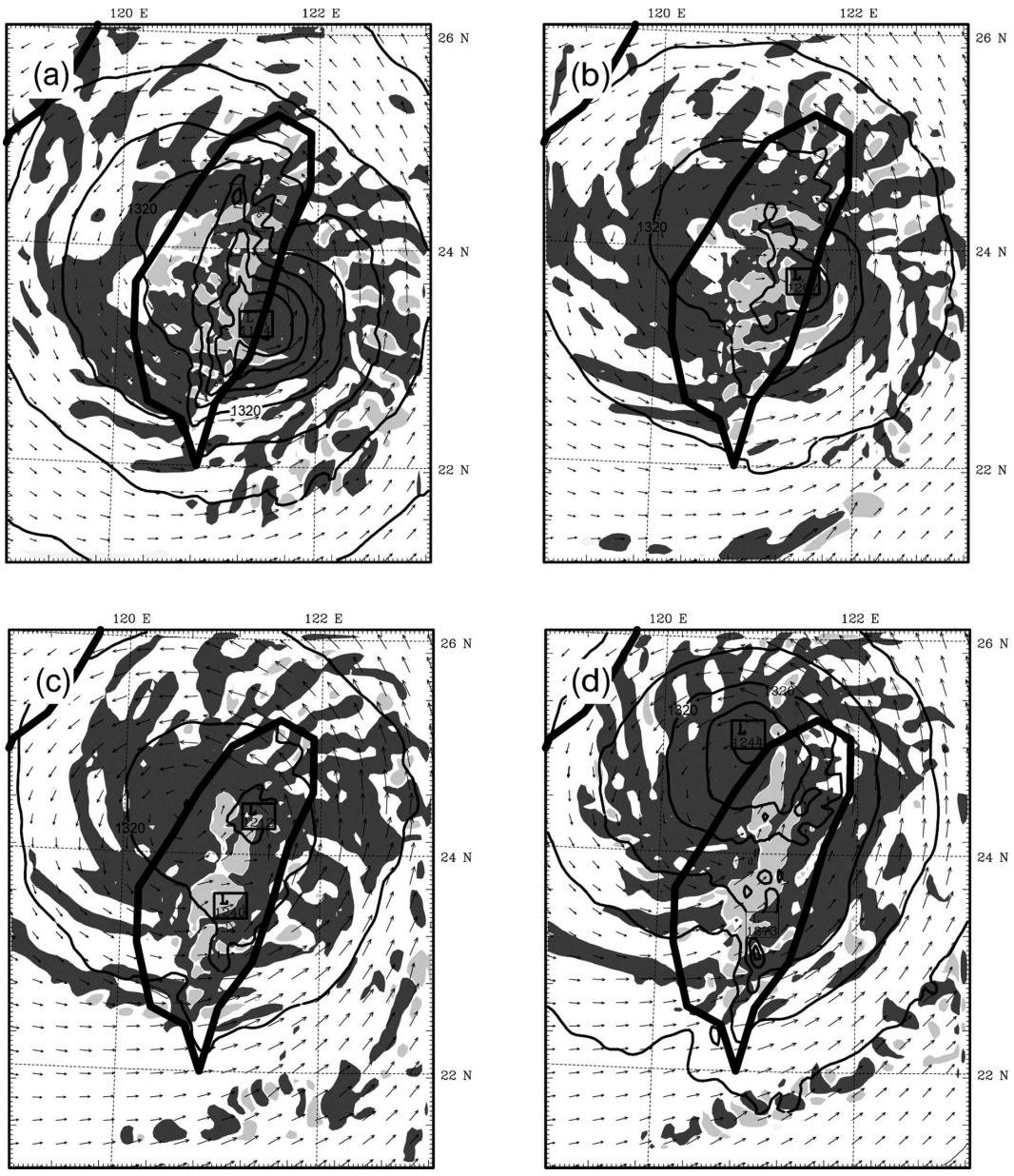

FIG. 23. The 850-mb geopotential height, PV, and wind vectors for Typhoon Toraji at (a) 1700, (b) 1900, (c) 2100, and (d) 2300 UTC 29 Jul 2001. Areas of PV > 1 PVU are denoted by dark gray, while areas of PV < -1 PVU are denoted by light gray. (1 PVU $= 10^{-6}$ m^2 s^{-1} K kg^{-1}.)

translation speed. In fast-moving TCs, *U/Nh* is large and the track tends to be continuous. For slowly (fast) moving TCs, *U/Nh* is small (large), and the track tends to be discontinuous (continuous). The parameter $V_{\max}/Nh$ can be physically regarded as the vortex Froude number of the airstream associated with the typhoon tangential circulation. This number measures the ability of a tropical cyclone circulation to pass over a mountain. When $V_{\max}/Nh$ is large, more parcels within the TC circulation are able to cross over the mountain. With a weaker TC, the parcels cannot cross over the mountain, and the flow is blocked. In the case of Taiwan, the parcels tend to flow around the CMR. In this situation, the center either goes around the mountain or it reforms on the lee side, depending on where the TC impinges on the mountain. The parameter R/L_y is a ratio of the size of the TC versus the length of the mountain chain. A smaller TC encounters a stronger orographic blocking and thus a discontinuous track results when R/L_y is small. When R/L_y is moderate to

large, as in larger TCs, the track tends to be continuous since the air parcels are able to be advected around the northern tip of CMR, as in Taiwan's case. Control parameters U/fL_x and V_{max}/fR represent Eulerian and Lagrangian Rossby numbers, respectively, and h/L_x represents the mountain slope steepness.

Under the situation with discontinuous track, a secondary cyclone develops on the lee side of the mountain range and eventually replaces the parent cyclone, as has been observed in reality. Dynamically, this implies that strong (weak) orographic blocking will lead the cyclone track to be discontinuous (continuous). Orographic blocking will result in greater deflection of the moving cyclone to the left or right. In cases featuring very strong blocking, with very small values of V_{max}/Nh, U/Nh, R/L_y, U/fL_x, and V_{max}/fR, and a very large value of h/L_x, a westward-moving cyclone will tend to be deflected southward.

Although in principle, all the above six nondimensional parameters play roles in controlling the track deflection and continuity for cyclones crossing over a mesoscale mountain, LCHH found that the track continuity is controlled more by V_{max}/Nh and R/L_y and the degree of deflection is controlled more by U/Nh for TCs over Taiwan's CMR. Figure 24 shows continuous and discontinuous tracks in the parameter space of (U/Nh, V_{max}/fR, h/L_x, R/L_y) versus V_{max}/Nh, based on idealized simulations with a simple model performed in LCHH.

b. *Application of control parameters for track continuity and deflection to Bilis and Toraji*

Based on the numerical simulations of Bilis and Toraji, the dimensional flow parameters are estimated to be (V_{max}, U, N, R) = (i) (65 m s^{-1}, 8 m s^{-1}, 0.01 s^{-1}, 50 km) for Bilis; and (ii) (50 m s^{-1}, 5.9 m s^{-1}, 0.01 s^{-1}, 50 km) for Toraji. The orographic parameters are assumed to be (h, L_x, L_y) = (3 km, 80 km, 240 km) and $f = 5.8 \times 10^{-5}$ s^{-1}. Based on these dimensional parameters, we obtain (V_{max}/Nh, U/Nh, R/L_y, V_{max}/fR) = (i) (2.17, 0.27, 0.21, 22.4) for Bilis; and (ii) (1.67, 0.20, 0.21, 20.6) for Toraji. The steepness of CMR is h/L_x = 0.0375.

In Fig. 24, the nondimensional control parameters of Bilis and Toraji are estimated and denoted by "B" and "T," respectively. Compared with the regime diagram of (V_{max}/Nh, U/Nh; Fig. 24a) proposed by LCHH, clearly Bilis belongs to the regime of continuous track, while Toraji belongs to the regime of discontinuous track. Note the estimated vortex Froude number (V_{max}/Nh) is 1.67 for Toraji, which falls very close to the upper boundary of the critical zone of V_{max}/Nh = 1.6. In addition, the estimated V_{max}/fR exceeds the parameter space laid out for idealized numerical simulations performed in LCHH. This is due to the fact that as latent heating effects were not included in that study, simulated cyclone vortices were prescribed with relatively large radii of maximum wind (R), in order to ensure barotropic stability with the simulated vortex. In general, the simulated results appear to be consistent with the theory proposed in LCHH. As seen in the low-level wind vector field (Fig. 21c), the remnant of the low-level vortex of Toraji was blocked, dissipated, and a new one formed on the lee side. In addition, based on the above estimated control parameters and the flow regimes proposed by LCHH, Bilis and Toraji will turn to north upstream (east) of CMR. This is consistent with observations.

6. Concluding remarks

In this study, we used a nonhydrostatic mesoscale model (MM5) to simulate Supertyphoon Bilis (2000) and Typhoon Toraji (2001) and investigated the dynamics of track deflection caused by the CMR of Taiwan. The MM5 predicted the track of each storm reasonably well. For Bilis, the center made landfall in southeast Taiwan and made a cyclonic track over the CMR, similar to that found in previous studies. Bilis was stronger in strength and had a relatively faster forward motion. This helped preserve the vertical integrity of the cyclone center as it crossed the CMR and to make the track continuous. The use of a "bogus" vortex in the initialization process helped to produce a storm closer to the observed strength. Bilis is a classic example of a typhoon crossing Taiwan with a continuous track.

For comparison, we also studied Typhoon Toraji, a typical typhoon having a discontinuous track. Toraji was weaker and had a relatively slower forward speed that prevented the original low center from surviving the trip across the CMR, and forced more air parcels to go around the northern tip of CMR. This produced a secondary lee vortex and generated downslope winds north of the center and a secondary low center. From the streamline and geopotential height analyses, one can clearly see a new low-level center forming in northwest Taiwan even before the primary center made landfall. The PV banners on the north side of the CMR acted to organize the secondary low and the vortex. Over time, the low-level circulation extended into the upper levels, completing the formation of the secondary center. Remnants of the initial upper-level center crossed over the CMR and were entrained into the secondary center.

The formation of the secondary low was examined

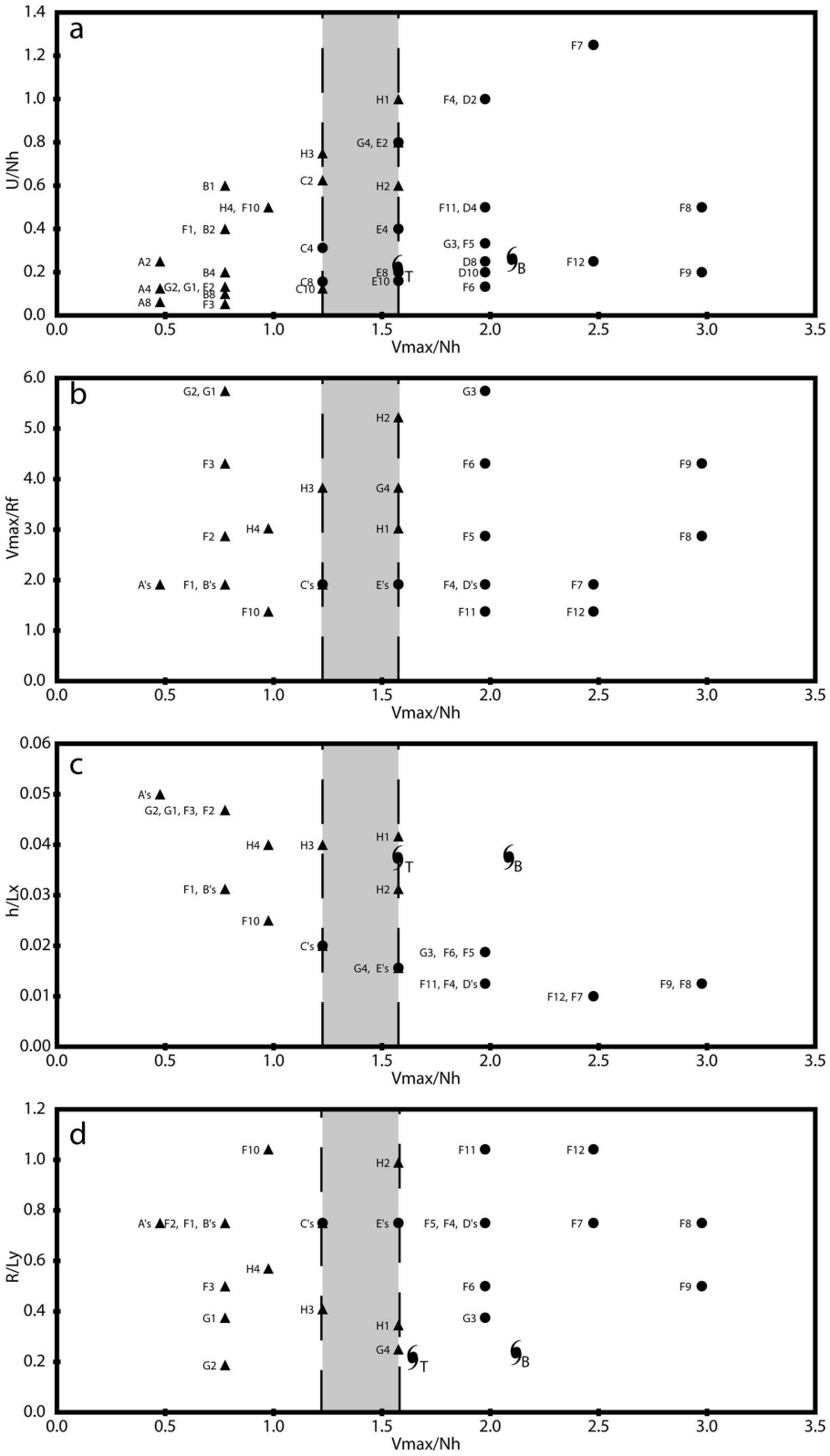

FIG. 24. Continuous (triangles) and discontinuous (circles) tracks in the parameter spaces of (U/Nh, V_{max}/fR, h/L_x, R/L_y) vs V_{max}/Nh, based on idealized simulations of LCHH. The proposed critical zone for cyclone track continuity is denoted by the gray-shaded block. Parameters of Bilis and Toraji are denoted as B and T, respectively, in the parameter spaces.

for Toraji. The first step in the low formation is from the adiabatic warming, which occurs in the lee of the CMR. This warming produced an area of lower heights to the north of the original typhoon center and west of the CMR. For a weaker TC, such as Toraji, the pressure depression generated by the adiabatic warming can be of a similar magnitude to that of the primary center. As the primary center impinges on the CMR, it is weakened, and the secondary low is allowed to take over. For Toraji, the entrainment of PV banners from the north side of the CMR into the secondary circulation center appears to help make it the dominant center over time. More research is needed to see if this process occurs in other typhoons. In Bilis, the strength and forward speed prevented the formation of a significant secondary low.

Based on the numerical simulations of Bilis and Toraji, the nondimensional flow parameters are estimated to be (V_{max}/Nh, U/Nh, R/L_y, V_{max}/fR) = (i) (2.17, 0.27, 0.21, 22.4) for Bilis; and (ii) (1.67, 0.20, 0.21, 20.6) for Toraji. The steepness of CMR is h/L_x = 0.0375. Compared with the regime diagram of (V_{max}/Nh, U/Nh) proposed by LCHH, clearly Bilis belongs to the regime of continuous track, while Toraji belongs to the regime of discontinuous track. In general, the simulated results appear to be consistent with the theory proposed in LCHH. In addition, based on the above estimated control parameters and the flow regimes proposed by LCHH, Bilis and Toraji will turn to north upstream (east) of CMR. This is also consistent with observations.

For TCs approaching Taiwan from the southeast, LCHH proposed a conceptual model for continuous and discontinuous tracks which is shown in Fig. 25. For a continuous track (Fig. 25a), the circulation remains vertically coupled at all levels. Weak secondary lows may form in the lee of the CMR, but the primary circulation remains intact after crossing the CMR. The kinetic energy associated with the original center is sufficiently high to allow the center to cross the CMR remaining intact. For continuous tracks over the CMR, the blocking effect on the outer circulation of the vortex is weak and the vorticity advection around the northern tip is strong as a result of an intense TC. TCs with moderate intensity will tend to have a discontinuous track (Fig. 25b). With these TCs, the blocking is moderate. The original center weakens as it crosses the CMR while a new center forms in the lee of the CMR from adiabatic warming and PV advection. Weak TCs tend to be totally blocked by the CMR (Fig. 25c). The primary low weakens and dissipates as it impinges on the CMR. A combination of adiabatic warming from downslope winds and the formation of vorticity fila-

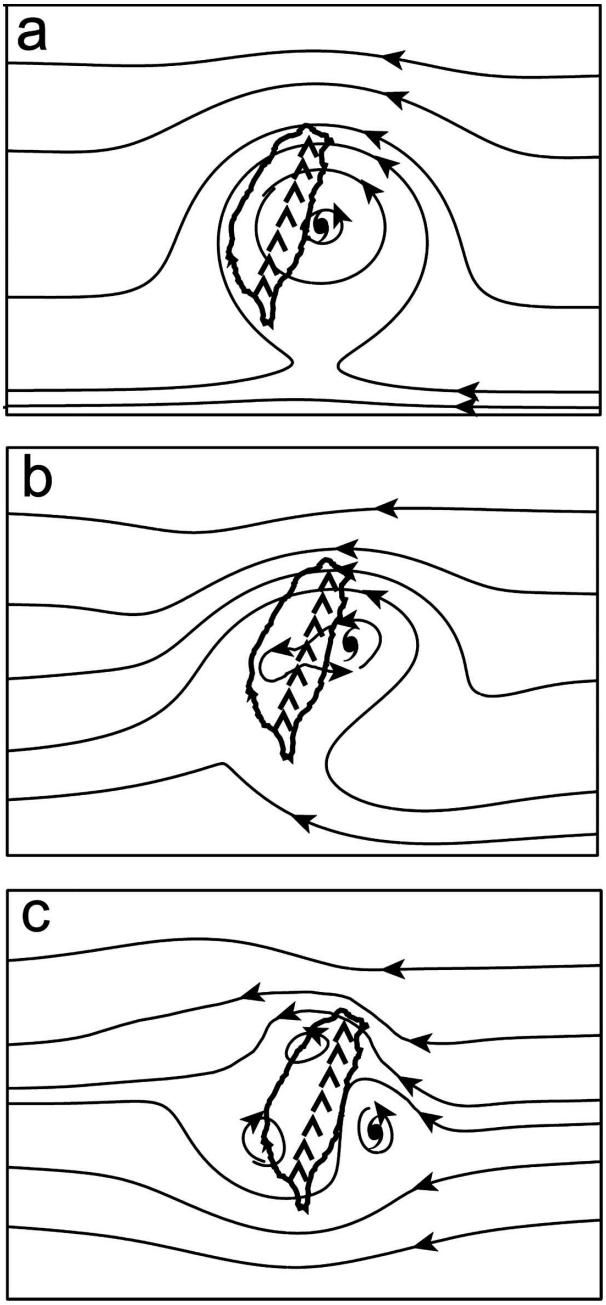

FIG. 25. A conceptual model depicting three different responses of a westward-propagating cyclone to orographic forcing by the CMR: (a) weak blocking: the cyclone is deflected slightly northward upstream of the CMR, and deflected back to the south after crossing the CMR, leading to a continuous track; (b) moderate blocking: the cyclone is deflected northward upstream of the CMR, while a secondary vortex forms in the lee of the CMR due to adiabatic warming and vortex stretching of the outer circulation of the cyclone, leading to a discontinuous track; and (c) strong blocking: similar to (b) except that the cyclone is deflected to the south and a secondary cyclone is developed at the northwest slope of the CMR. This leads to a discontinuous track. The strength of the blocking by the CMR is dependent on the intensity and forward speed of the cyclone. (Adapted from LCHH.)

ments as the low-level flow is deflected around the north side of the CMR help to generate a stronger secondary low on the northwest slope of the CMR, which ultimately becomes the primary low center. Bilis appears to be most similar to the schematic in Fig. 25a, while Toraji falls somewhere between Figs. 25b,c.

In future studies we plan on calculating vorticity and potential vorticity budgets for the TCs in this study, as well as other TCs. Similar calculations have been performed on idealized simulations (see Lin et al. 1999), and it will be interesting to see if similarities can be found with real and theoretical cases. The budget calculations will allow us to examine the physical mechanisms involved for lee cyclogenesis for discontinuous cyclone tracks across the CMR, as well as track deflections for continuous cyclone tracks. Effects of planetary boundary layer, latent heating, impinging angles, and landfalling locations need to be further investigated to fully understand the dynamics.

Acknowledgments. The authors would like to express their appreciation to G. M. Lackmann, C.-Y. Huang, C.-C. Wu, and S.-T. Wang for valuable comments on this study. Dr. Sen Chiao's help on the numerical modeling simulations is highly appreciated. Mesoscale analysis provided by the Central Weather Bureau of Taiwan is greatly appreciated. This work is partially funded by NSF Award INT-0129369 under NSF-UCAR Cooperative Agreement ATM-973265, NSF ATM-0344237, and ONR Grant N00014-02-1-0674.

REFERENCES

Bender, M. A., R. E. Tuleya, and Y. Kurihara, 1985: A numerical study of the effect of a mountain range on a landfalling tropical cyclone. *Mon. Wea. Rev.,* **113,** 567–582.

——, ——, and ——, 1987: A numerical study of the effect of island terrain on tropical cyclones. *Mon. Wea. Rev.,* **115,** 130–155.

Betts, A. K., and M. J. Miller, 1993: The Betts-Miller scheme. *The Representation of Cumulus Convection in Numerical Models, Meteor. Monogr.,* No. 46, Amer. Meteor. Soc., 107–121.

Brand, S., and J. W. Blelloch, 1974: Changes in the characteristics of typhoons crossing the island of Taiwan. *Mon. Wea. Rev.,* **102,** 708–713.

Chang, S. W.-J., 1982: The orographic effects induced by an island mountain range on propagating tropical cyclones. *Mon. Wea. Rev.,* **110,** 1255–1270.

Grell, G. A., J. Duhdia, and D. R. Stauffer, 1994: A description of the fifth-generation Penn State/NCAR Mesoscale Model (MM5). NCAR Tech. Note 398, 121 pp.

Huang, C.-Y., and Y.-L. Lin, 1997: The evolution of mesoscale vortex impinging on symmetric topography. *Proc. Natl. Sci. Council,* **21A,** 285–309.

Jian, G.-J., C.-S. Lee, and G. T.-J. Chen, 2006: Numerical simulation of Typhoon Dot (1990) during TCM-90: Typhoon Dot's discontinuous track across Taiwan. *Terr. Atmos. Oceanic Sci.,* **17,** 23–52.

Lin, Y.-L., 1993: Orographic effects on airflow and mesoscale weather systems over Taiwan. *Terr. Atmos. Oceanic Sci.,* **4,** 381–420.

——, R. D. Farley, and H. D. Orville, 1983: Bulk parameterization of the snow field in a cloud model. *J. Climate Appl. Meteor.,* **22,** 1065–1092.

——, J. Han, D. W. Hamilton, and C.-Y. Huang, 1999: Orographic influence on a drifting cyclone. *J. Atmos. Sci.,* **56,** 534–562.

——, D. B. Ensley, S. Chiao, and C.-Y. Huang, 2002: Orographic influences on rainfall and track deflection associated with the passage of a tropical cyclone. *Mon. Wea. Rev.,* **130,** 2929–2950.

——, S.-Y. Chen, C. M. Hill, and C.-Y. Huang, 2005: Control parameters for the influence of a mesoscale mountain range on cyclone track continuity and deflection. *J. Atmos. Sci.,* **62,** 1849–1866.

Low-Nam, S., and C. Davis, 2001: Development of a tropical cyclone bogussing scheme for the MM5 system. Preprints, *11th PSU–NCAR Mesoscale Model Users' Workshop,* Boulder, CO, PSU–NCAR, 130–134.

Schär, C., and R. B. Smith, 1993a: Shallow-water flow past isolated topography. Part I: Vorticity production and wake formation. *J. Atmos. Sci.,* **50,** 1373–1400.

——, and ——, 1993b: Shallow-water flow past isolated topography. Part II: Transition to vortex shedding. *J. Atmos. Sci.,* **50,** 1401–1412.

——, and D. R. Durran, 1997: Vortex formation and vortex shedding in continuously stratified flows past isolated topography. *J. Atmos. Sci.,* **54,** 534–554.

Smith, R. B., and D. F. Smith, 1995: Pseudoinviscid wake formation by mountains in shallow-water flow with a drifting vortex. *J. Atmos. Sci.,* **52,** 436–454.

Tao, W.-K., and J. Simpson, 1993: The Goddard cumulus ensemble model. Part I: Model description. *Terr. Atmos. Oceanic Sci.,* **4,** 35–72.

Wang, S.-T., 1980: Prediction of the movement and strength of typhoons in Taiwan and its vicinity. Research Rep. 108, National Science Council, Taipei, Taiwan, 100 pp.

Wu, C.-C., 2001: Numerical simulation of Typhoon Gladys (1994) and its interaction with Taiwan terrain using the GFDL hurricane model. *Mon. Wea. Rev.,* **129,** 1533–1549.

——, and Y.-H. Kuo, 1999: Typhoons affecting Taiwan: Current understanding and future challenges. *Bull. Amer. Meteor. Soc.,* **80,** 67–80.

Yang, M.-J., and L. Ching, 2005: A modeling study of Typhoon Toraji (2001): Physical parameterization sensitivity and topographic effect. *Terr. Atmos. Oceanic Sci.,* **16,** 177–213.

Yeh, T.-C., and R. L. Elsberry, 1993a: Interaction of typhoons with the Taiwan orography. Part I: Upstream track deflections. *Mon. Wea. Rev.,* **121,** 3193–3212.

——, and ——, 1993b: Interaction of typhoons with the Taiwan orography. Part II: Continuous and discontinuous tracks across the island. *Mon. Wea. Rev.,* **121,** 3213–3233.

Zhang, D., and R. A. Anthes, 1982: A high-resolution model of the planetary boundary layer—Sensitivity tests and comparisons with SESAME-79 data. *J. Appl. Meteor.,* **21,** 1594–1609.